Atmos. Chem. Phys. Discuss., 10, 21791–21866, 2010
www.atmos-chem-phys-discuss.net/10/21791/2010/
doi:10.5194/acpd-10-21791-2010

Atmospheric Chemistry and Physics Discussions

The Chemistry of Atmosphere-Forest Exchange (CAFE) Model – Part 2: Application to BEARPEX-2007 observations

G. M. Wolfe[1,2], J. A. Thornton[2], N. C. Bouvier-Brown[3,*], A. H. Goldstein[3], J.-H. Park[3], M. McKay[3,], D. M. Matross[3,***], J. Mao[4,****], W. H. Brune[4], B. W. LaFranchi[5,*****], E. C. Browne[5], K.-E. Min[5], P. J. Wooldridge[5], R. C. Cohen[5], J. D. Crounse[6], I. C. Faloona[7], J. B. Gilman[8,9], W. C. Kuster[8], J. A. de Gouw[8,9], A. Huisman[10], and F. N. Keutsch[10]**

[1]Department of Chemistry, University of Washington, Seattle, WA, USA
[2]Department of Atmospheric Sciences, University of Washington, Seattle, WA, USA
[3]Department of Environmental Science, Policy, and Management, University of California, Berkeley, CA, USA
[4]Department of Meteorology, Pennsylvania State University, University Park, PA, USA

[5]Department of Chemistry, University of California, Berkeley, CA, USA
[6]Division of Chemistry and Chemical Engineering, California Institute of Technology, Pasadena, CA, USA
[7]Department of Land, Air and Water Resources, University of California, Davis, CA, USA
[8]NOAA Earth System Research Laboratory, Boulder, CO, USA
[9]Cooperative Institute for Research in Environmental Sciences, University of Colorado, Boulder, CO, USA
[10] Department of Chemistry, University of Wisconsin, Madison, WI, USA
[*]now at: Chemistry and Biochemistry Department, Loyola Marymount University, Los Angeles, CA, USA
[**]now at: California Air Resources Board, Sacramento, CA, USA
[***] now at: KEMA, Inc., Oakland, CA, USA
[****]now at: School of Engineering and Applied Sciences, Harvard University, Cambridge, MA, USA
[*****] now at: Center for Accelerator Mass Spectrometry (CAMS), Lawrence Livermore National Lab, Livermore, CA, USA

Received: 24 August 2010 – Accepted: 5 September 2010 – Published: 20 September 2010

Correspondence to: J. A. Thornton (thornton@atmos.washington.edu)

Published by Copernicus Publications on behalf of the European Geosciences Union.

Abstract

In a companion paper, we have introduced the Chemistry of Atmosphere-Forest Exchange (CAFE) model, a vertically-resolved 1-D chemical transport model designed to probe the details of near-surface reactive gas exchange. Here, we use CAFE to interpret noontime observations from the 2007 phase of the Biosphere Effects on Aerosols and Photochemistry Experiment (BEARPEX-2007), conducted at a young Ponderosa pine plantation in the western Sierra Nevada. The model reproduces many features of the BEARPEX-2007 data and offers new insights into the forest-atmosphere exchange of reactive molecules at this location. Nitrogen oxide ($NO_x = NO + NO_2$) fluxes are driven by soil emissions of NO, while the partitioning between NO and NO_2 fluxes is sensitive to in-canopy photochemical gradients. Enhanced thermolysis at the ground increases downward acyl peroxy nitrate (APN) fluxes by as much as 50%, in general agreement with previous findings. APN fluxes are also influenced by in-canopy chemical production, especially when their formation is tied closely to oxidation of BVOC emissions. Gross dry N deposition is typically dominated by nitric acid, though other reactive nitrogen (NO_y) species can comprise up to 28% of the N deposition budget under cooler conditions. Upward NO_2 fluxes cause the net above-canopy NO_y flux to be ~30% lower than the gross depositional flux. Model-measurement comparison of hydrogen peroxide mixing ratios suggests this molecule deposits at the aerodynamic limit. CAFE under-predicts ozone fluxes by ~20%, which may indicate additional in-canopy chemical losses that are missing from the current model.

1 Introduction

Forest-atmosphere exchange of hydrocarbons, ozone, oxidized nitrogen and other reactive species impacts both atmospheric composition and ecosystem productivity, with broad implications for air quality and climate (Goldstein et al., 2009; Isaksen et al., 2009; Fowler et al., 2009; Erisman et al., 1998). Quantifying deposition and emission

ACPD
10, 21791–21866, 2010

to/from the forest, however, continues to present a significant experimental and theoretical challenge. Recent work has indicated that the air within and just above the canopy is highly oxidizing during the daytime (Farmer and Cohen, 2008; Holzinger et al., 2005; Lelieveld et al., 2008). This oxidative photochemistry affects the net biosphere-atmosphere exchange of many species. For example, the "escape efficiency" of highly reactive terpenoids is likely much less than unity (Ciccioli et al., 1999; Stroud et al., 2005; Bouvier-Brown et al., 2009a; Forkel et al., 2006), with consequences for scaling up leaf-level emissions for use in regional and global models. As a substantial in-canopy sink for oxidants like O_3, this chemistry could also contribute to downward O_3 fluxes (Goldstein et al., 2004; Kurpius and Goldstein, 2003; Fares et al., 2010).

Chemistry can also influence surface fluxes of reactive nitrogen compounds, including NO_x ($= NO + NO_2$), acyl peroxy nitrates (APNs), alkyl nitrates (ANs) and nitric acid (HNO_3). Several measurement and modeling studies have demonstrated the influence of in-canopy gradients in radiation, O_3 and turbulent transport on fluxes of NO_x (Gao et al., 1991; Dorsey et al., 2004; Duyzer et al., 2004). One set of observations showing upward HNO_3 and APN fluxes over a young Ponderosa pine plantation suggests that, under certain conditions, intra-canopy chemistry may even alter the sign of fluxes traditionally assumed to be controlled by deposition (Farmer and Cohen, 2008). More recently, Wolfe et al. (2009) observed downward APN fluxes at the same forest, but determined that the magnitude of the flux was sensitive to multiple in-canopy processes, including deposition, thermal decomposition and photochemical production.

The complexity of the forest-atmosphere interface introduces an array of potential biosphere-atmosphere feedbacks that are sensitive to temperature, radiation, atmospheric composition and other parameters that can change sharply in the vertical (Fowler et al., 2009; Fuentes et al., 2001). Numerical modeling is thus an ideal tool for examining the interplay of physical and chemical processes contributing to net reactive gas exchange. We employ the Chemistry of Atmosphere-Forest Exchange (CAFE) model in conjunction with the comprehensive dataset from the Biosphere Effects on Aerosols and Photochemistry Experiment (BEARPEX) 2007 field campaign

ACPD
10, 21791–21866, 2010

to investigate forest-atmosphere exchange at a young Ponderosa pine plantation. To our knowledge, CAFE is the first model of its kind to incorporate the extensive master chemical mechanism (MCM) for quantifying the chemical contributions to fluxes over forested regions. In Sect. 2 we briefly describe BEARPEX-2007 and review key features of CAFE. Section 3 presents an evaluation of observations from BEARPEX-2007, with a focus on the mechanisms controlling concentrations and fluxes of VOCs, hydrogen oxides, ozone, and reactive nitrogen.

2 Methods

2.1 Campaign and site description

BEARPEX-2007 was a multi-institutional collaborative research effort aimed at understanding the impact of forest-atmosphere interactions on atmospheric composition (Cohen et al., 2010). During the intensive measurement period of 15 August to 10 October 2007, a wide suite of chemical and meteorological observations were obtained within and immediately above a 17-year-old Ponderosa pine plantation managed by Sierra Pacific Industries. The site is adjacent to the University of California's Blodgett Forest Research Station (BFRS), located in the western foothills of the Sierra Nevada Mountains, CA (38°58′42.9″ °N, 120°57′57.9″ °W, elevation 1315 m), and has been described in detail elsewhere (Goldstein et al., 2000). The BFRS overstory is primarily Ponderosa pine, with a few interspersed White fir, Douglas fir, Incense cedar, Black oak and Sugar pine, while the understory consists of Manzanita and Ceanothus shrubs.

For the current study, we simulate mean noontime (11:30–12:30 PST) observations from two sub-periods, designated "hot" (28 August–3 September, or day of year 240–246) and "cool" (13–18 September, or day of year 256–261). These windows were chosen because day-to-day meteorology (particularly temperature) is fairly uniform throughout each period, and because they contain the most overlap among chemical observations. Figure 1 illustrates near-surface temperature profiles for each period.

ACPD
10, 21791–21866, 2010

The hot and cool periods are representative of the general meteorological trend observed during BEARPEX-2007, characterized by a hot and dry August followed by a sharp transition to cooler, more humid conditions in September (Bouvier-Brown et al., 2009a; Wolfe et al., 2009); however, neither period is representative of the extreme conditions sampled during the campaign. Both periods are largely cloud free and remain under drought conditions, as the selected cool period precedes the first rain. Chemical observations from these periods are discussed in Sect. 3.

2.2 Model description

CAFE is a 1-D chemical transport model that resolves deposition, emission, chemistry and vertical diffusion throughout the canopy and mixed layer. The CAFE model is described in detail in a companion paper (Wolfe and Thornton, 2010), and we will only briefly review the key aspects and modifications here. Table 1 lists important model parameters. The model domain consists of 86 layers in the vertical ranging from 0.01 m to 800 m, with non-even layer spacing that results in a fine-resolution grid of 36 layers within the forest canopy and 50 within the atmospheric boundary layer (ABL). The modeled canopy includes (i) an overstory with a height of 10 m, a one-sided leaf area index (LAI) of 3.2 $m^2\,m^{-2}$ and a leaf area dry mass (d) of 219 $g\,m^{-2}$, and (ii) an understory with a height of 2 m, an LAI of 1.9 $m^2\,m^{-2}$ and a d of 377 $g\,m^{-2}$. The leaf area density function (LADF) mimics observed vertical vegetation structures (L. Misson, personal communication, 2008). Meteorological constraints are taken as the mean noontime observations from the hot and cool period, listed in Table 2, with further parameterizations as outlined in the description paper. Within each layer, the 1-D time-dependent continuity equation is solved to determine the rate of change for all chemical species:

$$\frac{\partial C(z)}{\partial t} = P(z) + L(z) + E(z) + D(z) + A(z) - \frac{\partial F(z)}{\partial z} \quad (1)$$

ACPD
10, 21791–21866, 2010

Terms on the right respectively represent rates of chemical production, chemical loss, emission, deposition, advection (horizontal mixing) and vertical turbulent flux divergence.

Turbulent diffusion is represented using a first-order flux-gradient approach:

$$\frac{\partial F(z)}{\partial z} = -\frac{\partial}{\partial z}\left(K(z)\frac{\partial C(z)}{\partial z}\right) \quad (2)$$

Above 12.5 m, the eddy diffusion coefficient, $K(z)$, is based on values used by Gao et al. (1993), scaled to an ABL height of 800 m. Below 12.5 m, $K(z)$ is a function of friction velocity and canopy height and includes a correction factor to account for "near-field" effects of canopy elements on eddy diffusion (Makar et al., 1999; Raupach, 1989), though the latter is close to unity for the current study. The resultant canopy residence time is ~2 min for our conditions (Wolfe and Thornton, 2010).

Emissions of biogenic VOC (BVOC), including 2-methyl-3-buten-2-ol (MBO), isoprene (C_5H_8), methyl chavicol (MCHAV, also known as estragole), and a suite of speciated monoterpenes (MT) and sesquiterpenes (SQT), are modeled in each canopy layer as a function of leaf density, light, temperature and vegetation type (overstory and understory). For each emitted compound and in each layer, the emission rate is calculated in units of molecules $cm^{-3}\,s^{-1}$ as

$$E(z) = E_b C_L(z) C_T(z)\left(d\frac{\mathrm{LADF}(z)}{\mathrm{LAI}}\right) \quad (3)$$

E_b is the basal emission rate in molecules per gram of leaf per second, $C_L(z)$ and $C_T(z)$ are dimensionless correction factors for light and temperature (Guenther et al., 1995), and the rightmost terms collectively represent the vertically-distributed leaf dry mass in grams of leaf per cubic centimeter. Basal emission rates are within the range of values reported for this forest (Bouvier-Brown et al., 2009b, c; Harley et al., 1998; Schade et al., 2000) and are adjusted to optimize model-measurement agreement during the hot period. Temperature and light corrections are taken from the literature (Bouvier-Brown et al., 2009c; Guenther et al., 1995; Harley et al., 1998). Speciated MT emissions

ACPD
10, 21791–21866, 2010

include α-pinene, β-pinene, limonene, 3-carene, myrcene, camphene, terpinolene, α-terpinene and γ-terpinene. SQT include α-bergamotene (ABERG), β-caryophyllene (BCARY), α-farnesene (AFARN) and unspeciated SQT (USQT). USQT are a proxy for the non-speciated SQT observations reported by Bouvier-Brown et al. (2009a, c). Soil NO emissions are parameterized a function of temperature assuming dry soil (Yienger and Levy, 1995; Williams et al., 1992) with a basal NO emission factor of 3 ngN m^{-2} s^{-1}. This gives temperature-corrected NO emission fluxes of 3.0 and 2.4 ngN m^{-2} s^{-1} for the hot and cool periods, respectively.

Deposition is calculated for 35 species using a standard resistance parameterization (Wesely, 1989; Zhang et al., 2003; Wesely and Hicks, 2000) and includes transfer across the laminar sublayer, stomatal and non-stomatal (e.g. cuticular) uptake, and ground deposition. The stomatal resistance calculation includes environmental corrections for light extinction, temperature and vapor pressure deficit (Zhang et al., 2003) and is optimized to agree with observationally-constrained, "top-down" calculations of stomatal resistance during BEARPEX-2007. Deposition resistances ($R_{dep}(z)$) for each species are calculated separately for the overstory and understory in each layer and scaled by LADF to give a first-order loss rate constant within each vertical layer:

$$k_{dep}(z) = \frac{\mathrm{LADF}(z)_{os}}{R_{dep}(z)_{os}} + \frac{\mathrm{LADF}(z)_{us}}{R_{dep}(z)_{us}} \quad (4)$$

Multiplication of $k_{dep}(z)$ by a concentration yields the first-order loss rate due to deposition in each layer.

Chemistry in CAFE is based on a subset of the Master Chemical Mechanism (MCM) version 3.1 (http://mcm.leeds.ac.uk/MCM/) that includes all reactions stemming from oxidation of MBO, isoprene, α-pinene, β-pinene, propanal (C_2H_5CHO) and methane. MCM names and structures for key species mentioned in this study are listed in Appendix A. Our mechanism also includes several modifications and additions to the base MCM, most of which are described in the companion paper. Notably, CAFE incorporates a suite of 36 additional reactions for the initial oxidation of monoterpenes, sesquiterpenes and MCHAV by OH, O_3 and NO_3. Products of these reactions include

ACPD
10, 21791–21866, 2010

(i) small oxidized VOC, such as formaldehyde and acetone, with yields as reported by laboratory oxidation studies (Atkinson and Arey, 2003; Lee et al., 2006a, b),

(ii) hydroxyl (OH) radicals from ozonolysis reactions, also with literature-reported yields (Atkinson and Arey, 2003; Lee et al., 2006a), and

(iii) the generic peroxy radicals MTO_2 and $SQTO_2$. The latter react with NO, HO_2 and RO_2 to form the species MTOX and SQTOX, which represent first-generation oxidation products of MT (excluding α-pinene and β-pinene) and SQT. Since these products are likely semi-volatile and their detailed chemistry is presently unknown, MTOX and SQTOX are given a deposition velocity equal to that of nitric acid (near the aerodynamic limit) and do not undergo further reactions.

CAFE also incorporates isoprene dihydroxyepoxide chemistry (Paulot et al., 2009c) and assumes that the epoxide (IEPOX) deposits at the aerodynamic limit.

For the current investigation, we incorporate one significant modification to the mechanism described in Wolfe and Thornton (2010). When VOC emissions are high (i.e. during the hot period), an additional "enhanced OH recycling" mechanism is required to bring modeled OH values into agreement with measurements. We employ a mechanism of the type

$$RO_2 + HO_2 \xrightarrow{k_{rec}} \alpha OH + \text{products} \quad (5)$$

where α is a stoichiometric constant. These reactions, listed in Table 3, are implemented only for first-generation MBO and isoprene-derived peroxy radicals (RO_2 = $MBOAO_2$, $MBOBO_2$, ISOPAO2, $ISOPBO_2$, $ISOPCO_2$ and $ISOPDO_2$). The reaction "products" are those of the decomposition of the corresponding RO radicals, which are explicitly tracked. Values for α and k_{rec} are tuned to optimize model-measurement agreement for OH and HO_2; for the current study, we choose $\alpha = 2.6$ and $k_{rec} = 4.5 \times 10^{-11}$ cm^3 molec^{-1} s^{-1}. We discuss and evaluate the consequences of this mechanistic change further in Sect. 3.2.

ACPD
10, 21791–21866, 2010

Advection is treated as a simple mixing process in each model layer with a mixing rate constant (k_{mix}) of 0.3 hr^{-1} (Dillon et al., 2002; Perez et al., 2009):

$$\left(\frac{dC}{dt}\right)_{mix} = -k_{mix}(C - C_a) \quad (6)$$

Advection concentrations (C_a) are set constant throughout the model domain but are different for the hot and cool periods (Table 4). The primary role for this scheme is to maintain reasonable concentrations for species that would otherwise build up to unreasonable values or decay below measured values during integration. Advection thus allows us to better constrain CAFE to BEARPEX-2007 observations. We will note when this term influences the interpretation of results.

For each period, meteorological observations (Table 2) are used to initialize diffusion parameters, emission rates, deposition velocities and chemical rate constants, which are held constant throughout a model run. Initial/advection chemical concentrations for each period (Table 4) are chosen to optimize model-measurement agreement. Integration is accomplished via operator splitting, using a Crank-Nicolson scheme to solve the diffusion operator and a forward Euler scheme for the chemical operator (Jacobson, 2005). Soil NO emission and ground deposition are incorporated into the diffusion operator, while canopy emissions, deposition and advection are represented in the chemistry operator. The model is run for two hours, which is sufficient time for relaxation of exchange velocity profiles. Fluxes and exchange velocities are calculated from concentration profiles at the end of a model run via

$$F(z) = -K(z)\frac{\Delta C(z)}{\Delta z} \quad (7)$$

$$V_{ex}(z) = F(z)/C(z) \quad (8)$$

ACPD
10, 21791–21866, 2010

3 Results and discussion

Here, we compare CAFE model output with observations from the BEARPEX-2007 field campaign. Table 5 lists a selection of chemical observations for each period. Quoted measurement values are the means and standard deviations of 30-min averaged data. The hot period is typified by relatively high concentrations of BVOC, HO_x, O_3 and oxygenated hydrocarbons and lower levels of NO_2 and acyl peroxy nitrates (APN = PAN + PPN + MPAN + ...); cold period data demonstrate the opposite trends. Differences in local atmospheric composition between the hot and cool periods are largely driven by temperature (as opposed to wind direction, for example), which controls emission rates and subsequent photochemistry. Model results are examined with a particular focus on BVOC, RO_x ($= OH + HO_2 + RO_2$), hydrogen peroxides, O_3 and reactive nitrogen (NO_y). We evaluate modifications implemented in the CAFE model (e.g. OH recycling) and provide an assessment of the relative contributions of deposition, emission and chemistry to above-canopy chemical fluxes for key species. Unless otherwise specified, model results discussed below are extracted from two "base" model runs, one each for the hot and cool periods. The base run for the hot period is carried out with the OH-recycling mechanism, while the base cold period run does not include OH-recycling. The reasons for this choice are detailed in Sect. 3.2.

Reproducing observed concentrations is important for examining chemical contributions to fluxes, but we caution that the model is not strictly tailored towards reproducing all aspects of the chemistry (e.g. diurnal cycles) or, more importantly, transport. Modeled mixing ratios are, in a sense, constrained to the observations via the advection term and the initial/advection concentrations. We run CAFE in this fashion because our primary goal is to understand the observed fluxes, though we also point out other interesting features in the model-measurement comparison when they arise. Modeled concentration and fluxes should not be taken as representative of daily or seasonal "average" conditions, but rather as mid-day "snapshots" from the two periods. An extended comparison table of modeled and measured concentrations can be found in Appendix B.

ACPD
10, 21791–21866, 2010

3.1 VOC

Within and immediately above the forest, concentrations of primary BVOC (MBO, isoprene, MCHAV, MT and SQT) are controlled by relative rates of emission and oxidation. Calculation of "bulk canopy" emission rates provides a means for validation of vertically-resolved emissions. Taking MBO as an example: integration of the hot-period MBO emission rate over the canopy height gives a bulk emission rate of 5.2×10^{11} molec cm^{-2} s^{-1} (1.9 mgC m^{-2} h^{-1}), or a boundary-layer average of 6.6×10^{6} molec cm^{-3} s^{-1}. These rates are within the range of previous MBO flux measurements at BFRS (Baker et al., 1999; Schade et al., 2000) and of values employed by other models (Perez et al., 2009; Steiner et al., 2007).

Isoprene is not emitted in significant quantities from Ponderosa pine, Manzanita or Ceanothus (Bouvier-Brown, personal communication, 2009), but it can originate from less abundant vegetation within the forest stand and upwind, particularly Black Oak. Although direct measurements of above-canopy isoprene fluxes have not been conducted at BFRS, early isoprene gradient measurements and relaxed eddy accumulation observations in 1998 and 1999 indicated no significant emissions from BFRS (Dreyfus et al., 2002; Goldstein et al., 2001). Analysis of mixing ratio diurnal profiles at this site have determined that isoprene is primarily advected from a band of Oak located 30–40 km upwind (Dreyfus et al., 2002). The current construction of CAFE is unable to simultaneously reproduce the concentrations of isoprene and its main oxidation products, methyl vinyl ketone (MVK) and methacrolein (MACR), solely through our advection scheme. Thus, in addition to advecting isoprene at a rate of 1 ppbv hr^{-1}, we invoke a substantial emission rate of isoprene ($\sim$ 40% of the MBO emissions). While local (e.g. $<$ 500 m upwind) isoprene emissions are likely smaller than modeled in CAFE, our isoprene emission rate is nearly identical to that used in the 4 km $\times$ 4 km grid cell of a three-dimensional model that contains BFRS (Steiner et al., 2007). The vertical profile of isoprene, and potentially its oxidation products, will depend somewhat on the nature of its sources (i.e. emission vs. advection). A small set of in-canopy isoprene

ACPD
10, 21791–21866, 2010

gradients measured near the end of the BEARPEX-2007 campaign (after our cool period) suggest that in-canopy isoprene mixing ratios can exceed above-canopy values by as much as a factor of 2 (data not shown), but it remains unclear if this gradient can be attributed to local emissions. In what follows, we will note when this issue affects our conclusions.

Though our emissions estimates agree with other literature values, the standard emission parameterization does have limitations. Previous work at BFRS has shown that basal emission rates vary with water stress, temperature history and other factors (Gray et al., 2006, 2003) and that tree-to-tree variability in emission rates can be substantial (Bouvier-Brown et al., 2009c). Schade et al. (2000) also note that the top-down radiation attenuation algorithm, used to derive radiation correction factors for MBO and isoprene emissions, is not optimized for coniferous forests.

Since modeled mixing ratios of locally emitted BVOC are primarily a function of the rates of emission and chemical loss (e.g. advection often plays a small role), it is worthwhile to compare modeled and measured concentrations of these as done in Table 6. MBO and isoprene mixing ratios are reproduced to within 25% or better during both hot and cool periods, suggesting that the radiation and temperature adjustments are accurate for emissions of these compounds. MCHAV and MT are predicted to within 10% during the hot period but are under-predicted during the cool period by 60–70%, while SQT are over-predicted by 150%. These errors likely stem from the temperature corrections for emission rates, which become increasingly important at lower temperatures. Even though total MT concentrations are well reproduced during the hot period, modeled terpene speciation differs from observations. The model generally under-predicts β-pinene, limonene, 3-carene and USQT, and over-predicts myrcene, camphene, terpinolene, α-terpinene and γ-terpinene (Appendix B). Such discrepancies may arise from inaccurate estimates of emission speciation. Though we use the best estimates from a previous investigation (Bouvier-Brown et al., 2009c), terpene emissions are subject to plant physiological and environmental conditions that are not easily modeled. The relative terpene speciation has little impact on our conclusions

ACPD
10, 21791–21866, 2010

regarding the chemical contribution to trace gas fluxes. The terpene oxidation tracers MTOX and SQTOX show roughly the same seasonal trend as their VOC precursors (Table 6). Despite a fast deposition velocity, concentrations of MTOX and SQTOX build up to 101 and 41 pptv, respectively, during the hot period. Many of the compounds represented by these tracers will contain alkenyl moieties and thus may still play an important role in oxidative chemistry. For both periods, near-surface MTOX and SQTOX gradients (not shown) match earlier model results (Wolfe and Thornton, 2010).

In addition to the speciated single-height measurements, the BEARPEX-2007 dataset also includes vertical profiles of several classes of VOC acquired via proton-transfer mass spectrometry (PTR-MS). Details regarding instrumentation and measurement setup can be found elsewhere (Bouvier-Brown et al., 2009b; Holzinger et al., 2005). In Fig. 2, we compare modeled BVOC profiles to four sets of PTR-MS measurements: the sum of MBO and isoprene, the sum of MVK and MACR, total monoterpenes (Σ MT) and MCHAV. For clarity, observations and model results shown in Fig. 2 are from the hot period only and have been normalized to their canopy-top values; modeled and measured profiles exhibit similar normalized gradients for both the hot and cool periods. Model-measurement agreement is generally quite good, though the model tends to under-predict gradients of Σ MT and MCHAV in the lower canopy. Potential explanations include:

(i) emissions of these compounds from the understory are underestimated by CAFE, though these are mostly constrained by branch enclosure experiments (Bouvier-Brown et al., 2009c),

(ii) there is an unidentified emission source near the ground, such as decaying pine needles, as suggested by Stroud et al. (2005), or

(iii) turbulent mixing in the lower canopy is less efficient than parameterized here, which could lead to a buildup of BVOC emitted from the understory.

This last possibility would also be consistent with model-measurement comparisons of NO_2 and PAN (see Sect. 3.5). The mean observed MBO + isoprene mixing ratio at

ACPD
10, 21791–21866, 2010

$z/h = 0.15$ (1.5 m) is consistently 15% lower than that at 6.1 m. This feature persists even in individual 30-min gradient observations. As MBO (and isoprene, in CAFE) are primarily emitted from the overstory, this feature would also be consistent with a depositional sink of MBO and isoprene in a vertically stagnant layer near the ground (Stroud et al., 2005). The modeled MBO + isoprene profile might be less steep if isoprene were primarily advected in CAFE, as the isoprene profile would then be more vertical and observed isoprene mixing ratios are typically 30–50% of MBO at noon (Table 6). Even in such a case, however, we would still expect a somewhat negative in-canopy isoprene gradient due to lower OH mixing ratios within the canopy. Profiles of the sum of MVK and MACR, which are first-generation oxidation products of isoprene, are fairly vertical in both the model and measurement, reflecting that mixing of these compounds is faster than their production and loss. Previous studies have suggested that MVK and MACR should also deposit to the canopy/ground with a deposition velocity of 0.2–0.5 cm s^{-1} (Stroud et al., 2005; Zhang et al., 2003), which we do not include in CAFE.

The hydroxyl radical (OH) is the primary daytime oxidant for most VOC in the troposphere. OH reactivity (τ_{OH}^{-1}), or inverse lifetime, is defined as the sum of all OH loss rates divided by the OH concentration:

$$\tau_{OH}^{-1} = \sum_i k_i C_i \quad (9)$$

where k_i is the second-order rate constant for reaction of OH with species i having concentration C_i. OH reactivity was measured directly during BEARPEX-2007 following the approach described in Mao et al. (2009) and is useful for constraining both VOC inventories and steady-state calculations of oxidant concentrations. Figure 3 compares model calculations of τ_{OH}^{-1} with observed values. During the hot period, modeled (13.1 s^{-1}) and measured (12.4 ± 2.0 s^{-1}) τ_{OH}^{-1} are in excellent agreement. About 63% of the modeled τ_{OH}^{-1} is attributed to primary VOC, with another 22% due to reactions with HCHO, CO, CH_4 and the first-generation oxidation products of isoprene (MVK and MACR) and MBO (IBUTALOH and $HOCH_2CHO$). The remaining 15% ("other") includes

ACPD
10, 21791–21866, 2010

$\sim$300 reactions, each of which comprise $<1\%$ of τ_{OH}^{-1}. During the cool period, modeled τ_{OH}^{-1} ($3.7\,s^{-1}$) is lower than observations ($6.8 \pm 1.2\,s^{-1}$) by almost a factor of 2. This discrepancy cannot be explained by model underestimates of MT and MCHAV mixing ratios during this period but might be partly attributed to a missing formaldehyde (HCHO) source (Choi et al., 2010). These results, including the "missing OH reactivity" during the cold period, are consistent with observationally-constrained bottom-up estimates of τ_{OH}^{-1} (Mao et al., 2008). The latter study also demonstrates that measured anthropogenic VOC are a negligibly small contribution to τ_{OH}^{-1} at BFRS.

During the cool period, CAFE predicts HCHO mixing ratios of ~ 1.3 ppbv, while measurements indicate a noontime mean of 12.5 ± 4.0 ppbv (Appendix B); HCHO observations were not available during the hot period. Increasing HCHO mixing ratios to match observations (by raising the initial/advection HCHO concentrations) brings the modeled OH reactivity to $6\,s^{-1}$, which is within the range of observations. Maintaining this level of HCHO in the model leads to a 50% over-prediction of hydroperoxy radical (HO_2) and hydrogen peroxide (H_2O_2); OH increases by 15%. The sources of the elevated HCHO mixing ratios observed during the cold period are presently unknown but may be linked to oxidation of yet-unidentified reactive BVOC inferred from previous observations at BFRS (Choi et al., 2010; Holzinger et al., 2005). As constraining HCHO to measured values does not noticeably perturb the exchange velocities of key species in the model, we retain the CAFE-predicted HCHO values.

3.2 RO_x

Cycling of hydrogen oxide radicals is driven by VOC and nitric oxide (NO). The sequence begins with reaction of OH and VOC to produce an organic peroxy radical (RO_2). Subsequent reaction of RO_2 with NO produces NO_2 and an alkoxy radical (RO). Typically, the latter reacts with O_2 to yield a hydroperoxy radical (HO_2) and a closed-shell aldehyde or ketone. In the CAFE mechanism, the latter two processes are combined. OH is regenerated upon reaction of HO_2 with NO to form NO_2.

ACPD
10, 21791–21866, 2010

$$OH + VOC \rightarrow RO_2 + H_2O \quad (10)$$

$$RO_2 + NO \rightarrow NO_2 + HO_2 + \text{carbonyls} \quad (11)$$

$$HO_2 + NO \rightarrow OH + NO_2 \quad (12)$$

As a result of this cycling, we define the chemical families $HO_x = OH + HO_2$, $RO_x = HO_x + RO_2$ and $NO_x = NO + NO_2$. Partitioning within the RO_x and NO_x families is thus coupled by VOC abundance and reactivity with OH. Moreover, cross-reactions between RO_x and NO_x produce longer-lived reactive nitrogen species, the forest-atmosphere exchange of which can be sensitive to vertical gradients in this chemistry.

Figure 4 depicts modeled profiles of OH, HO_2 and RO_2 radicals. For each period, the model was run both with and without the enhanced OH recycling mechanism discussed in Sect. 2.2. Both periods show small positive (increasing with height) in-canopy HO_2 gradients of ∼5%. The OH mixing ratio increases by ∼10% between the ground and the top of the canopy in the hot period and by ∼40% in the cool period. The relative gradients are mostly unaffected by the enhanced OH-recycling mechanism, though OH does exhibit a slight bulge maximizing at $z/h = 1.4$ during the hot period with enhanced OH recycling, and RO_2 is ∼20% higher within the canopy than above for the same scenario. We now discuss our choice to implement an enhanced OH recycling method for the purposes of providing reasonable model estimates of in-canopy oxidation processes.

Model-measurement mismatch of OH is a recurrent issue in investigations of RO_x chemistry under conditions where BVOC such as isoprene are a dominant source of RO_2 (Hofzumahaus et al., 2009; Lelieveld et al., 2008; Thornton et al., 2002; Ren et al., 2008; Martinez et al., 2003; Tan et al., 2001). Many of these studies, and others, have proposed mechanisms to augment radical production and propagation, including

(i) reduction in the formation rate of isoprene-derived organic hydroperoxides and/or enhancement of their photolysis rates (Thornton et al., 2002),

ACPD
10, 21791–21866, 2010

(ii) additional production of OH during reactions of isoprene-derived first-generation RO_2 with HO_2 (Lelieveld et al., 2008; Thornton et al., 2002),

(iii) inclusion of an unknown species "X" that reacts with RO_2 and HO_2 with the same efficacy as NO (Hofzumahaus et al., 2009), and

(iv) RO_2 isomerization and decomposition (Peeters et al., 2009; Da Silva et al., 2010).

We tested each of these mechanisms separately in CAFE, but found that no single mechanism could adequately reproduce observed HO_x partitioning and abundance simultaneously with other key indicators, such as oxidized VOC abundance and speciation. For example, incorporation of the isoprene hydroxyperoxy radical isomerization/decomposition mechanism – as implemented in Stavrakou et al. (2010) with an OH yield of 3 from the photolysis of hydroxyperoxy aldehyde products – leads to a 30% over-prediction of HO_2 but a factor of three under-prediction of OH in the hot period. The postulated isomerization requires an allylic radical, thus first-generation MBO-derived peroxy radicals will not undergo analogous reactions. As MBO is the dominant VOC at BFRS, this mechanism alone cannot fully explain model-measurement discrepancies in HO_x.

During the hot period, enhanced OH recycling is critical for replicating observations. Excluding this mechanism leads to under-prediction of noontime OH by a factor of 6 and of HO_2 by ~25%; RO_2 was not measured. Using measured OH reactivity and concentrations, and assuming OH is in steady state (i.e. production equals loss), we estimate an observationally-constrained gross OH production rate (P_{OH}) of ~4 pptv s^{-1} for noontime conditions during the hot period. Without OH recycling, modeled P_{OH} for the hot period is ~0.7 pptv s^{-1} and is mainly driven by O_3 photolysis and reaction of HO_2 with NO. As the model accurately reproduces measured OH reactivity during the hot period (Fig. 3), we conclude that the under-prediction of OH stems from inefficient recycling and/or excessive termination by RO_x cross-reactions. Inclusion of the tuned OH recycling mechanism (Table 3) brings modeled OH and HO_2 to within the range of observations and increases RO_2 by a factor of 3. HO_2 is both a reactant

ACPD
10, 21791–21866, 2010

and product in the enhanced OH-recycling mechanism, thus the increase in modeled HO_2 is primarily due to a larger source from RO_2 reactions with NO. Another potentially important OH source is ozonolysis of highly-reactive VOC not included in our emission inventory (Goldstein et al., 2004; Holzinger et al., 2005; Faloona et al., 2001). Holzinger et al. (2005) estimated that an average in-canopy O_3 reaction rate of 5.25×10^8 molec cm^{-3} s^{-1}, or 25 pptv s^{-1}, would be required to sustain the chemical contribution to in-canopy ozone fluxes inferred by previous studies (Goldstein et al., 2004; Holzinger et al., 2005; Kurpius and Goldstein, 2003). Given that our missing P_{OH} is $\sim$3.3 pptv s^{-1}, an average OH yield of 13% from these reactions would be sufficient to sustain measured OH levels, at least in the canopy. The resulting OH concentration from such a source, however, would lead to model overestimates of HO_2 (and likely RO_2). That is, such a source would still imply an incomplete understanding of RO_2/HO_2 chemistry.

Our enhanced OH-recycling mechanism is similar to a blending of those proposed by Lelieveld et al. (2008) and Peeters et al. (2009). Our mechanism ties OH recycling to $RO_2 + HO_2$ reactions, but it is an additional process in competition with the peroxide-forming channel. The mechanism also simultaneously converts the primary MBO and isoprene-derived RO_2 radicals into the relevant oxidation products as if passing through the respective RO radicals. Essentially, it is an enhanced RO_2 decomposition that yields OH and oxidized VOC but has little net effect on HO_2. Failure to incorporate RO_2 destruction in the enhanced OH recycling mechanism leads to unrealistic RO_2 concentrations (> 300 pptv), which in turn results in overestimation of several oxidation products – such as glyoxal and acetone – and underestimation of the NO/NO_2 ratio. With our enhanced OH recycling mechanism, model results are consistent with RO_2 and NO/NO_2 values derived from observationally-constrained steady-state calculations for this site (LaFranchi et al., 2009; Day et al., 2008) and with observations of total peroxy radicals at other forested locations (Cantrell et al., 1992; Qi et al., 2005). Furthermore, small-chain BVOC oxidation products agree reasonably well with BEARPEX-2007 observations (Appendix B), though mixing ratios of these are

ACPD
10, 21791–21866, 2010

also influenced by advection. Previous studies at BFRS have provided evidence for a temperature-dependent HO_x source (Day et al., 2008; Farmer and Cohen, 2008). The OH production rate from our enhanced recycling mechanism is also consistent with this observational evidence as it decreases with decreasing temperature by virtue of its reliance on RO_2 formed from BVOC.

In contrast to the hot period, modeled OH agrees with observations during the cool period without the need for additional OH recycling, while HO_2 is somewhat underpredicted. As CAFE underestimates measured OH reactivity by a factor of 2 during the cool period, however, this agreement is likely artificial. Incorporating enhanced OH recycling during the cool period leads to overestimation of OH by a factor of ~ 2; thus, by constraining modeled OH reactivity to the measured value and assuming the reactivity is caused by a non-methane hydrocarbon that is not MBO or isoprene, model-measurement agreement of OH concentrations during the cool period can be achieved with the enhanced recycling mechanism. As this result ultimately depends on the nature of the missing reactivity, and as OH, HO_2, and RO_2 abundances are reasonably predicted by CAFE during the cool period without the recycling mechanism, we leave this issue for future investigation.

3.3 Peroxides

In high-RO_x and high-VOC environments, peroxide formation is considered a key radical termination step:

$$HO_2 + HO_2 \rightarrow H_2O_2 + O_2 \quad (13)$$

$$RO_2 + HO_2 \rightarrow ROOH + O_2 \quad (14)$$

In the case of isoprene oxidation, further reaction of first-generation ROOH with OH can generate dihydroxyepoxides (Paulot et al., 2009c):

$$ROOH + OH \rightarrow IEPOX + OH \quad (15)$$

ACPD
10, 21791–21866, 2010

Comparison of modeled and measured peroxides/epoxides thus provides an additional indirect check on RO_x abundance and chemistry in CAFE. BEARPEX-2007 observations include both hydrogen peroxide (H_2O_2) and the sum of first-generation isoprene hydroxyhydroperoxides (ISOPOOH, see Appendix A) and isoprene dihydroxyepoxides (IEPOX).

As shown in Table 6, ISOPOOH+IEPOX is over-predicted by 23% during the hot period and under-predicted by 64% during the cool period. Constraining OH and isoprene to measured values without enhancing RO_2 destruction (as in our OH-recycling scheme) leads to a factor of two over-prediction of ISOPOOH + IEPOX. Under-prediction during the cool period is consistent with the underestimate of HO_2 and may also indicate under-prediction of RO_2 for this scenario. These compounds have been assigned initial/advection concentrations of 0 to simplify comparison to observations, though it is very likely that their "advection concentrations" are higher than we ascribe due to the upwind isoprene source. Increasing advection would degrade model-measurement agreement during the hot period and improve it during the cool period; however, modeled ISOPOOH + IEPOX mixing ratios are mostly controlled by chemical production/loss and deposition. Deposition rates for these compounds are also somewhat uncertain. Model-measurement agreement only changes slightly in the absence of ISOPOOH deposition, which is currently implemented with a deposition velocity of $\sim 1.6\,cm\,s^{-1}$ (Hall and Claiborn, 1997). IEPOX is forced to deposit at the aerodynamic limit in CAFE; neglecting IEPOX deposition entirely during the hot period increases the CAFE overestimate of ISOPOOH + IEPOX to 53%. Regardless, modeled ISOPOOH + IEPOX mixing ratios are within the observed variance of ± 60% during the hot period, suggesting that modeled isoprene-RO_2 concentrations – when using our enhanced OH-recycling mechanism – are reasonable for this scenario.

H_2O_2 concentrations are overestimated by 49% for the hot period and 21% for the cool period (Table 6) when the literature-recommended effective Henry's Law coefficient (H^*) of $1 \times 10^5\,M\,atm^{-1}$ (Seinfeld and Pandis, 2006) is used in the deposition parameterization. This implies a missing or underestimated H_2O_2 sink. Setting

ACPD
10, 21791–21866, 2010

$H^* = 1 \times 10^{14}$ M atm^{-1} yields above-canopy exchange velocities of −4 to −5 cm s^{-1} and improves agreement with observed mixing ratios. In this case, H_2O_2 concentrations are underestimated by 17% during the cool period, which is consistent with a 17% underestimate of HO_2 in this same period, though we caution that H_2O_2 mixing ratios are somewhat dependent on our choice of initial/advection concentrations (currently set to 0.8 ppbv for the cool period). Field studies elsewhere have reported diffusion-limited H_2O_2 deposition over forests, much faster than predicted by the Wesely (1989) parameterization (Ganzeveld et al., 2006; Hall and Claiborn, 1997). Recent measurements at BFRS also suggest transport-limited H_2O_2 deposition (Paulot et al., 2009a), a finding supported by our model results. Our choice to increase H^* to match the observed H_2O_2 exchange velocity does not necessarily imply that the molecular mechanism controlling H_2O_2 surface loss is related to solubility; rather, we view the cuticular resistance (which is controlled partly by H^*) as a tunable parameter that could represent any number of yet-undiscovered chemical or physical uptake processes.

3.4 Ozone

Deposition of O_3 is a major concern due to its deleterious effects on plant tissues (Darrall, 1989), which can reduce plant productivity (Sitch et al., 2007). Ozonolysis of reactive terpenoids generates OH as well as oxygenated VOC that may deposit to canopy surfaces or partition to secondary organic aerosol (Ciccioli et al., 1999; Holzinger et al., 2005). Such reactions are thought to alter the net forest-atmosphere flux of both O_3 and terpenoids (Goldstein et al., 2004; Kurpius and Goldstein, 2003; Stroud et al., 2005). Failure to account for such chemical effects could lead to errors when using above-canopy ozone flux measurements to assess O_3-induced ecosystem damage. Figure 5 compares model and measured O_3 concentrations, fluxes and exchange velocities. Mixing ratios agree reasonably well, showing slight positive gradients in the canopy region. Modeled downward (negative) fluxes and exchange velocities fall within the variability of observations but tend to under-predict mean values by ∼20% for both

ACPD
10, 21791–21866, 2010

periods. CAFE successfully predicts the observed 20% increase in O_3 fluxes between the hot and cool period, which is due to a small decrease in the stomatal resistance accompanying the reduced vapor pressure deficit and temperature (Table 2). This behavior is counter to the generally-positive correlation between temperature and O_3 fluxes observed on longer timescales at BFRS but is within the variability of measured O_3 fluxes from a 6-year dataset (Fares et al., 2010).

Previous work at BFRS has provided evidence that both deposition (stomatal and non-stomatal uptake) and in-canopy reactions with biogenic emissions, particularly MT and SQT, can influence O_3 fluxes (Goldstein et al., 2004; Kurpius and Goldstein, 2003; Fares et al., 2010). It is thus prudent to examine all processes contributing to O_3 fluxes, defined by the various terms in the mass balance equation (Eq. 1). Figure 6a shows vertically-resolved instantaneous rates for all processes during the hot period. The model predicts that deposition is the dominant factor within the canopy region. Other factors are small but consistent with expected chemical behavior, which derives primarily from the NO_x-O_3 equilibrium:

$$NO_2 \xrightarrow{h\nu} O(^3P) + NO \quad (16)$$

$$O(^3P) + O_2 \rightarrow O_3 \quad (17)$$

$$NO + O_3 \rightarrow NO_2 + O_2 \quad (18)$$

Gross chemical O_3 production tracks light attenuation in the canopy, as it is rate-limited by NO_2 photolysis. Gross O_3 chemical loss is also primarily via photolysis in the top half of the canopy but increases near the ground due to reaction with soil-emitted NO. The net chemical tendency ($P + L$) changes sign halfway through the canopy. These results are consistent with those from other canopy models (Stroud et al., 2005). Contributions from advection (A) and $\partial C / \partial t$ are small.

The vertical flux at any height, $F(z)$, is the sum of the ground-up integrals of the rate of each process in Eq. (1):

ACPD
10, 21791–21866, 2010

$$F(z) = \underbrace{\int_0^z [E(z) + D(z)]dz}_{\text{Surf}} + \underbrace{\int_0^z \left[P(z) + L(z) + A(z) - \partial C(z)/\partial t\right] dz}_{\text{Chem}} \quad (19)$$

Here, we group contributions into surface and "chemical" processes (for O_3, $E(z) = 0$); these groups could also be thought of as "heterogeneous" and "gas phase." The integral over height of $\partial C/\partial t$ (the last term) is, by definition, the "storage" term employed in interpretation of flux observations (Rummel et al., 2007; Wolfe et al., 2009). Calculation of fluxes by this method yields the same values as those computed via Eq. (7), and normalization of each term by the modeled mixing ratio at any height gives the corresponding component of the exchange velocity. CAFE predicts that surface deposition controls the vertical flux of ozone (Fig. 6b). Chemistry induces a slight positive slope on the O_3 exchange velocity profile above the canopy, consistent with net production. Similar results are found for the cool period.

In Table 7, we list the various processes contributing to the total modeled O_3 exchange velocity ($V_{ex}(O_3)$). Stomatal uptake, which is constrained by independent calculations based on observed latent heat fluxes (Wolfe and Thornton, 2010), accounts for 46% and 59% of the modeled $V_{ex}(O_3)$ during the hot and cool periods, respectively. Non-stomatal (e.g. cuticular) and ground deposition comprise the remaining 54% and 41%. Modeled $V_{ex}(O_3)$, however, under-estimates the mean measured values by 24% and 20%. Moreover, our parameterization of cuticular and ground deposition likely over-estimates the magnitude of these processes at BFRS. Constraints for non-stomatal deposition in CAFE are taken from a "big leaf" resistance model (Zhang et al., 2003, 2002) that assumes similar values across a fairly wide swath of ecosystems, and unlike the stomatal component, there is no simple way to validate this parameterization against observations. The possible influence of intra-canopy chemistry on observed above-canopy O_3 fluxes was not considered during the development of these parameterizations. Detailed resistance models often include empirical adjustments to the cuticular resistance (R_{cut}) for friction velocity, humidity, solar radiation and other factors (Erisman et al., 1994, 2005), but it is not clear whether the true underlying mechanisms

ACPD
10, 21791–21866, 2010

are reactive uptake, gas-phase chemistry, or a combination of the two. In the extreme case where non-stomatal deposition is ignored, CAFE would under-predict observed O_3 fluxes by 65% and 53% for the hot and cool periods, respectively.

Within the current model framework, in-canopy O_3 + BVOC reactions are not of sufficient magnitude to influence O_3 fluxes, seemingly at odds with inferred non-depositional O_3 fluxes at BFRS (Kurpius and Goldstein, 2003; Goldstein et al., 2004). In these studies, the authors note that emissions of very reactive BVOC – which can drive chemical O_3 fluxes – may not be included in current emission inventories. Such emissions have also been postulated from observations of "missing" OH reactivity at a forest in northern Michigan (Di Carlo et al., 2004). For BEARPEX-2007, CAFE reproduces the observed above-canopy OH reactivity during the hot period (Fig. 3), when BVOC emissions are highest. Thus, to affect ozone fluxes, these unidentified emissions must react preferentially with O_3 in the canopy, similar to the SQT species β-caryophyllene and α-humulene (Bouvier-Brown et al., 2009c). The effects of very reactive BVOC on O_3 chemistry should be localized to the canopy or near-leaf airspace, consistent with the observation of markedly different terpene speciation between branch enclosure and ambient measurements (Bouvier-Brown et al., 2009a). CAFE already contains emissions of highly reactive SQT that account for some of the missing ozone reactivity inferred previously (Kurpius and Goldstein, 2003; Goldstein et al., 2004). Bringing our model results into agreement with these studies, however, would require a substantial increase in emissions of the highly reactive SQT species or other yet-unmeasured BVOC. Considerable non-stomatal ozone fluxes have been observed at several other forests (Hogg et al., 2007; Coe et al., 1995; Rondon et al., 1993), but whether such fluxes are driven by surface or gas-phase processes remains an open question. Targeted model sensitivity studies could shed further light on such issues. Understanding the fate of O_3 in the forest must continue to be a priority, as the questions raised here are directly relevant to ecosystem health, aerosol formation and RO_x chemistry in this environment.

ACPD
10, 21791–21866, 2010

3.5 Reactive nitrogen

The reactive nitrogen (NO_y) family encompasses a wide spectrum of atmospheric oxidized nitrogen compounds, including NO_x, acyl peroxy nitrates (APNs), alkyl nitrates (ANs) and nitric acid (HNO_3), among others. Primary NO_x sources in the troposphere include both anthropogenic (e.g. combustion and agriculture) and natural (e.g. soil and lightening) emissions (Jaeglé et al., 2005). The higher oxides of nitrogen are formed via reactions of NO_x with RO_x:

$$RC(O)O_2 + NO_2 \rightleftharpoons RC(O)O_2NO_2(APN) \quad (20)$$

$$RO_2 + NO \rightarrow RONO_2(AN) \quad (21)$$

$$OH + NO_2 \rightarrow HNO_3 \quad (22)$$

We restrict our analysis to these four classes since they comprise the bulk of NO_y at BFRS (Day et al., 2009; Ren et al., 2010) and their formation mechanisms are reasonably – if not yet quantitatively – understood. Table 8 compares modeled concentrations of NO_y components to observations. Overall, the model is in decent agreement with measured ΣNO_y ($= NO + NO_2 + \Sigma PN + \Sigma AN + HNO_3$) and the temperature-dependence of NO_y speciation, though ΣPN (comprised primarily of APNs in the model) are slightly over-predicted and ΣAN are slightly under-predicted. Speciation is discussed in more detail below. ΣNO_y measured during BEARPEX-2007 (1–1.3 ppbv) is about half that reported for previous years (~ 2.5 ppbv), but the relative speciation is similar (Day et al., 2009; Murphy et al., 2007).

Forest-atmosphere exchange of reactive nitrogen continues to be a significant uncertainty in assessing the influence of anthropogenic nitrogen emissions on forest productivity (Magnani et al., 2007; Thomas et al., 2010) and regional air quality (Steiner et al., 2006). Quantifying dry nitrogen deposition to forests remains a challenge because:

(i) deposition velocities may vary by an order of magnitude for different classes of NO_y (Farmer and Cohen, 2008; Turnipseed et al., 2006; Horii et al., 2006);

ACPD
10, 21791–21866, 2010

(ii) deposition can alter the relative partitioning of remaining gas-phase NO_y, which in turn affects NO_y chemistry and deposition downwind; and

(iii) rapid in-canopy chemical transformations can alter the net forest-atmosphere exchange of NO_y species (Dorsey et al., 2004; Duyzer et al., 2004; Farmer and Cohen, 2008; Walton et al., 1997; Wolfe et al., 2009).

Soil-emitted NO, often a primary NO_x source in rural and remote regions (Williams et al., 1992), is rapidly converted to NO_2 by reaction with O_3 and peroxy radicals in the canopy (Gao et al., 1991), with implications for measuring the fluxes of NO_x components. NO_x partitioning within the canopy also affects the fate of APNs, which depends in part on the NO/NO_2 ratio. Oxidation of BVOC can enhance or alter the pathways for production of APNs and ANs, while temperature gradients can influence the decomposition of APNs to NO_x, affecting fluxes of both of these components (Farmer and Cohen, 2008; Wolfe et al., 2009). In what follows, we examine the modeled vertical exchange for each class of NO_y with a focus on the role chemistry plays in modifying the net above-canopy flux.

3.5.1 NO_x

Figure 7a displays vertical profiles of NO_2 mixing ratios. NO_2 is lower during the hot period, likely because of faster conversion to HNO_3 and a decreased APN reservoir (Day et al., 2008). Concentrations increase near the ground due to fast conversion of soil-emitted NO via reactions with O_3 and peroxy radicals, as well as relatively enhanced thermolysis of APNs via the reverse of Eq. (20). The measured NO_2 gradient is steeper than the model during the hot period, which may be symptomatic of stagnant conditions in the lower canopy that are not accurately represented by our diffusion parameterizations. Gradients in the NO/NO_2 ratio (Fig. 7b) are driven by a balance between the soil NO emission rate, rapid establishment of the $NO\text{-}NO_2\text{-}O_3$ equilibrium reactions (Eqs. 16–18), and diffusion timescales. NO/NO_2 is lower during the hot period because of higher levels of RO_2, which mainly convert NO to NO_2 via Eq. (11) but also to ANs via Eq. (21).

ACPD
10, 21791–21866, 2010

The mirrored shape of in-canopy flux profiles (Fig. 7c–d) reflects the rapid interconversion of NO and NO_2. Near the ground, low radiation results in net conversion of emitted NO to NO_2, thereby increasing fluxes of NO_2 and decreasing those of NO. Flux profiles turn more vertical at $z/h \cong 0.6$, when NO_2 photolysis becomes competitive with NO oxidation. The net NO_x flux above the canopy is upward and nearly equal in magnitude to the soil NO emission flux, though it is mostly comprised of NO_2. NO_2 deposition (with a deposition velocity of $\sim 0.4\,cm\,s^{-1}$) and conversion to higher oxides of nitrogen decrease this flux slightly, but these effects are small for the current study. During the hot period, CAFE predicts an above-canopy NO_2 exchange velocity of $+3.5\,cm\,s^{-1}$, which is 50% higher than the $+2.3\,cm\,s^{-1}$ observed by Farmer and Cohen (2008) at BFRS in August 2004. If above-canopy NO_2 fluxes are a good indicator of the soil NO flux, as our results suggest, then we may be over-estimating the soil NO flux by 50%. This assumes, however, that conditions are similar between 2004 and 2007, and we have no direct constraint on the soil NO emission flux from either period.

3.5.2 APNs

APNs are a unique class of NO_y in that their atmospheric residence time, determined partly by the chemical equilibrium Eq. (20), is highly sensitive to temperature. Peroxyacetyl nitrate (PAN, $CH_3C(O)O_2NO_2$) is 70–90% of the observed APN budget during BEARPEX-2007 and evolves from a variety of anthropogenic and biogenic VOC precursors. Notable minor APNs include peroxypropionyl nitrate (PPN, $C_2H_5C(O)O_2NO_2$) and peroxymethacryloyl nitrate (MPAN, $CH_2C(CH_3)C(O)O_2NO_2$), which form during the oxidation of C_2H_5CHO and MACR, respectively. BEARPEX-2007 measurements (Table 5) include vertical concentration gradients and above-canopy fluxes of PAN, PPN and MPAN, as well as a separate measurement of total peroxy nitrates (ΣPN) that may contain contributions from other APNs and non-acyl species such as $CH_3O_2NO_2$. Most of our analysis will focus on the speciated observations, since these include fluxes.

ACPD
10, 21791–21866, 2010

After accounting for both thermal decomposition via the reverse reaction in Eq. (20) and subsequent loss of the $RC(O)O_2$ radical, canopy-top APN lifetimes for the current study range from ∼1.5 h during the hot period to ∼8 h during the cool period. Both observed and modeled PAN concentrations are lower during the hot period (Fig. 8a) despite higher concentrations of PAN precursors. PAN mixing ratios are over-predicted by ∼60% during the hot period but agree well with observations during the cool period. Model-measurement agreement for mixing ratios is partly coupled to our choice of PAN initial/advection concentrations (Table 4). This finding is somewhat consistent with the steady-state analysis of LaFranchi et al. (2009), who suggested that overestimates of modeled PAN during warmer conditions may have resulted from underestimated sinks for $CH_3C(O)O_2$ (PA) radicals. Additionally, our extensive chemical mechanism predicts several individually small sources of the PA radical, neglected by LaFranchi et al. (2009), that sum to ∼30% of the total PA production budget. In contrast, PPN and MPAN concentrations are in fair agreement with observations during both periods (Appendix B).

Model overestimates of ΣPNs (Table 8) are due, in part, to accumulation of several other APNs, specifically PHAN, C4PAN5, C4PAN6, C5PAN17 and C5PAN19 (see Appendix A), which together make up 37% of modeled ΣPNs during the hot period and 17% during the cool period. These compounds evolve during the first oxidation steps of MBO and isoprene. With the exception of PHAN (which was not calibrated), the UW-CIMS instrument did not detect a signal from these compounds during BEARPEX-2007 (Wolfe et al., 2009). As argued in Wooldridge et al. (2010), previous comparisons of ΣPN measurements by the UCB-TD-LIF instrument with speciated APN observations suggest that APNs other than PAN, PPN, and MPAN typically make up a very small fraction (< 10%) of ΣPNs. Possible explanations for the apparent over-prediction of these species by the MCM include (i) the presence of hydroxyl groups, which may enhance deposition relative to the modeled value, and/or (ii) enhanced unimolecular decomposition of the acyl peroxy radicals (Butkovskaya et al., 2006), which is not represented in our chemical mechanism. If modeled deposition rates are too slow for these

ACPD
10, 21791–21866, 2010

compounds, then the model is underestimating NO_y dry deposition. Conversely, if the model-measurement discrepancy is indicative of enhanced unimolecular decomposition rates for the acyl peroxy radicals, then the model may over-predict the contribution of ΣPNs to total NO_y deposition. The contribution of APNs other than PAN, PPN, and MPAN to dry N deposition ultimately depends on their concentrations and deposition velocities, both of which remain very uncertain; if constituting ∼37% or more of the total APN flux, however, these are clearly non-negligible.

Looking closer at the measured PAN gradient near the ground reveals that observations at 1.5 m are consistently lower than those at 5 m, with an average difference of 26 ± 14 pptv (mean $\pm 1\sigma$) between these two heights for the hot period (data not shown). This constitutes a gradient of $\sim 17 \pm 9\%$ that is not captured in the modeled PAN profile, suggesting the presence of additional losses near the ground not represented in CAFE. These losses may include enhanced deposition to surfaces (e.g. soil and ground litter). Alternatively, the steeper observed PAN gradient may result from retarded diffusion close to the ground, where chemical sinks are largest; we discuss this further below.

Modeled PAN fluxes and exchange velocities (Fig. 8b–c) are under-predicted by 50–60% for both periods. Deposition of PAN occurs primarily through stomatal uptake (Table 7). It is possible that non-stomatal deposition is under-predicted in CAFE, though laboratory measurements suggest that this term should be small compared to stomatal uptake (Sparks et al., 2008). The 22% decrease in the observed PAN exchange velocities (V_{ex}(PAN)) between the hot and cool periods suggests a temperature-dependent in-canopy loss process that is not represented in CAFE. Surface-facilitated thermal decomposition on sunlit canopy elements (which are warmer than the surrounding air) followed by loss of the PA radical seems a feasible mechanism, though the magnitude of this process would need to be larger than our total modeled deposition rate.

Alternatively, model-measurement disagreement may be related to gas-phase chemistry and vertical mixing. Enhanced thermal decomposition due to the strong temperature gradient at the ground (Fig. 1) forces PAN out of chemical equilibrium

ACPD
10, 21791–21866, 2010

(i.e. $P < L$), resulting in net chemical loss within the canopy and increasing its downward flux. This chemical perturbation, which we will call the chemical velocity (V_c) in analogy with the deposition velocity (V_d), comprises 45% and 31% of the modeled V_{ex}(PAN) during the hot and cool periods, respectively (Table 7). Wolfe et al. (2009) estimated an average V_c(PAN) of −0.3 and −0.1 cm s^{-1} for two larger periods of BEARPEX-2007 that include our hot and cool periods, respectively. Thus, it is possible that CAFE underestimates this effect, especially during the hot period. For example, the presence of a "stagnant" layer near the ground that is somehow decoupled from the upper canopy airspace would yield a longer residence time in this region, where chemical PAN losses are largest. This would exacerbate the effects of enhanced in-canopy chemical losses on PAN fluxes and possibly also help explain the observed PAN and NO_2 gradients discussed above. Altering the diffusion scheme in CAFE could provide a test of this hypothesis.

PPN and MPAN fluxes and exchange velocities (Table 9) are mostly within the large range of observed values, except for the PPN exchange velocity during the hot period. Measured PPN exchange velocities are quite fast (< −3 cm s^{-1}) during the hot period, the possible implications of which have been discussed elsewhere (Wolfe et al., 2009). Within the CAFE model framework, an exchange velocity of this magnitude can only be obtained if PPN deposition rates are increased markedly by decreasing the cuticular resistance. The high variability of PPN and MPAN exchange velocities for the chosen observation windows, however, precludes a more detailed model evaluation for these species.

Separating APN fluxes into chemical and surface (depositional) contributions can provide a more detailed look into the factors controlling forest-atmosphere APN exchange. Figure 9 compares the chemical velocities of PAN, PPN, MPAN and C4PAN5 for the hot period, as calculated from Eq. (19). The latter species is the primary first-generation APN from MBO oxidation as predicted by the MCM and is an analog of MPAN, which derives from isoprene. Even though we do not have observations for comparison, we include C4PAN5 in this analysis for demonstrative purposes. Starting

ACPD
10, 21791–21866, 2010

near the ground, V_c(PPN) diverges slightly towards less negative values than PAN, while V_c(MPAN) is even less negative. The chemical velocity of C4PAN5 shows the largest departure from PAN, becoming positive above $z/h = 0.5$. These variations are not due to differences in deposition, as all APNs have the same V_d in the model, also shown in Fig. 9 (though they may vary somewhat between species in reality).

The diversity of modeled APN chemical velocity profiles is largely due to varying vertical distributions of their precursors. This is particularly evident in MPAN and C4PAN5 chemical velocities. Near the ground, the chemical velocity of MPAN and C4PAN5 is still controlled by thermal losses. Within and immediately above the canopy, however, oxidation of emitted isoprene and MBO leads to formation of methacrolein (MACR) and 2-hydroxy-2-methylpropionaldehyde (IBUTALOH), respectively. In our MCM-based mechanism, these aldehydes are the sole precursors of MPAN and C4PAN5, respectively, and slightly enhanced levels of these precursors will enhance MPAN and C4PAN5 formation at the surface. This production term continues to grow above the canopy, whereas the thermochemical loss term becomes more constant as the temperature gradient is less pronounced here (note the near-vertical gradient of V_c(PAN) between $z/h = 1$ and 2). The magnitude of the modeled MPAN exchange velocity is reduced $\sim$50% at the APN flux observation height (17.8 m). V_c(C4PAN5) is strong enough that CAFE predicts net emission of this compound from the forest, though this prediction is sensitive to the deposition term, which may be higher than we have modeled due to the hydroxyl functionality on C4PAN5. BVOC oxidation also produces PAN precursors, but these are not as specific as those of MPAN and C4PAN5. PAN production includes significant contributions from multi-generational oxidized VOC, such as acetaldehyde and methyl glyoxal, that are not as directly linked to BVOC emissions and thus are more evenly distributed in the vertical. The PPN chemical velocity is slightly less negative than V_c(PAN) because of an increased contribution from the storage term, $-\int_0^z \frac{\partial C(z)}{\partial t} dz$. In this case, the PPN precursor propanal (C_2H_5CHO) is evenly distributed in the vertical because its sole source in CAFE is advection. PPN produced aloft is transported into the canopy but cannot escape as easily, as decreased diffusion

ACPD
10, 21791–21866, 2010

in the canopy can serve as a "trap" for gases with weak concentration gradients. This results in a slight buildup of PPN and thus a slight positive perturbation to the flux. Chemical flux contributions are slightly dampened during the cool period (not shown), though MPAN exchange velocities are still somewhat less negative than those of PAN and PPN (Table 9).

The strength of any APN production flux will depend on a number of factors, including BVOC emission rates, OH mixing ratios and canopy residence times. In particular, we noted earlier (Sect. 3.1) that a substantial isoprene emission rate is required to maintain agreement with isoprene observations, though previous studies have identified advection as the primary isoprene source at BFRS (Dreyfus et al., 2002). Replacing isoprene emission with advection would reduce the MPAN production flux and bring the modeled MPAN V_{ex} closer to that of PAN or PPN, because the source of MACR would no longer be elevated in the canopy. Likewise, thermochemical APN loss fluxes depend on both the absolute temperature and the shape the temperature gradient in the canopy, which may change dramatically between a young and open forest like BFRS and a more mature forest. Moreover, APN production and loss are also subject to NO_x concentrations and NO/NO_2 ratios. To expand the relevance of these findings to other ecosystems, future modeling work should probe the sensitivity of APN fluxes to such factors, particularly temperature gradients, BVOC emissions and soil NO emissions.

3.5.3 ANs

Alkyl nitrates ($RONO_2$) are formed as minor products during $NO + RO_2$ reactions Eq. (21), with typical branching ratios of 5–10% for AN formation (Atkinson and Arey, 2003). ANs are also produced during the oxidation of VOC by the nitrate radical (NO_3), though daytime NO_3 concentrations are generally too low to be important in this canopy. Recent work suggests that chemical mechanisms may be incomplete with regard to AN chemistry, particularly concerning their ability to "recycle" NO_x during oxidation by OH (Rollins et al., 2009; Perring et al., 2009a, b; Horowitz et al., 2007; Paulot et al., 2009b). Deposition of ANs is also poorly constrained by observations and may

ACPD
10, 21791–21866, 2010

depend on the functional form of the R-group. BEARPEX-2007 measurements are limited to ΣAN concentration profiles, though earlier observations at this forest have included ΣAN fluxes.

Figure 10a–c displays modeled mixing ratios, fluxes and exchange velocities for $MBOANO_3$, which is a first-generation oxidation product of MBO that comprises ~50% of the modeled AN budget. Concentrations are slightly higher during the hot period, consistent with the ΣAN observations (Table 7) and with faster formation rates due to higher OH and BVOC. Vertical concentration gradients for both periods are characteristic of strong deposition. Deposition velocities are tuned to match the value of 2.7 cm s^{-1} suggested by Farmer and Cohen (2008) by increasing the effective Henry's Law constant to 1×10^8 M atm^{-1}, effectively lowering the cuticular resistance. Deposition thus dominates the flux and exchange velocity profiles, with slightly less negative V_{ex} during the hot period due to less stomatal uptake. A small contribution from in-canopy production increases $MBOANO_3$ fluxes towards less negative values by ~10%. Chemistry-driven fluxes could become more important if deposition rates are lower than modeled – a distinct possibility considering the limited observational constraints on this process – or if AN yields are higher. Other primary ANs derived from local BVOC (i.e. $MBOBNO_3$ and the 4 isoprene-derived ANs, see Appendix A) exhibit the same vertical and seasonal patterns as $MBOANO_3$.

3.5.4 HNO_3

Dry deposition of gas-phase nitric acid is a primary pathway for atmosphere-to-ecosystem nitrogen transfer. HNO_3 adsorbs readily to most surfaces, thus deposition is assumed to proceed at the aerodynamic limit. This view is generally supported by inferential (e.g. flux-gradient) measurements of HNO_3 fluxes over forests (Horii et al., 2006; Pryor and Klemm, 2004; Sievering et al., 2001), which report deposition velocities ranging from 2 to 10 cm s^{-1}. Previous eddy covariance measurements at BFRS (prior to BEARPEX-2007) have reported HNO_3 deposition velocities of 3–4 cm s^{-1} during winter but have also offered evidence that fast intra-canopy chemistry can influence HNO_3

ACPD
10, 21791–21866, 2010

fluxes, even to the point of creating a net upward flux (out of the forest) during the summer (Farmer and Cohen, 2008).

Figure 11a–c illustrates modeled profiles of HNO_3 mixing ratios, fluxes and exchange velocities. HNO_3 concentrations are ~2 times higher during the hot period relative to the cool period, consistent with faster production via Eq. (22) due to more OH and larger local NO_x sources from soil-emitted NO and APN decomposition. Fluxes and exchange velocities are fast and essentially driven by deposition. As in the cases of O_3 and ANs, changes in stomatal uptake give rise to different exchange velocities between the hot and cool periods. Modeled HNO_3fluxes do include a small (~5%) positive contribution due to in-canopy reactions of soil-emitted NO.

3.5.5 Nitrogen deposition

Ecosystem-scale nitrogen deposition affects biosphere productivity and represents a major pathway by which anthropogenic emissions influence the environment. Dry deposition typically constitutes ~50% of total atmospheric N deposition, with the other half due to wet deposition (i.e. precipitation) (Bytnerowicz and Fenn, 1996; Sparks et al., 2008). Though HNO_3 is likely the dominant dry-depositing species, several studies have inferred that a significant fraction of the downward NO_y flux is comprised of species other than nitric acid (Horii et al., 2006; Sparks et al., 2008). As detailed by the above discussion, inferring gross N deposition rates from net NO_y fluxes without considering in-canopy chemistry can lead to errors.

Figure 12 summarizes modeled above-canopy ($z/h = 2$) NO_y fluxes. Gross NO_y deposition amounts to 24 and 15 pptv m s^{-1} (11 and 7 ngN m^{-2} s^{-1}) for the hot and cool periods, respectively. This is within the range of other estimates of N deposition to California forests (Bytnerowicz and Fenn, 1996; Herman et al., 2003). HNO_3 constitutes 86% of deposited NO_y during the hot period but only 72% during the cool period, owing to decreased HNO_3 and increased APN and NO_2 mixing ratios. For both periods, upward NO_2 fluxes (driven by soil NO emissions) decrease the net modeled NO_y flux

ACPD
10, 21791–21866, 2010

by ∼30% relative to the gross deposition flux. Differences between total and depositional fluxes for individual classes of NO_y are consistent with our earlier discussion. For example, APN fluxes are only 60% depositional during the hot period, while total AN fluxes underestimate the depositional flux by ∼10%. Note that our analysis is focused on gaseous oxidized nitrogen and thus does not consider dry deposition of ammonia (NH_3) or particulate ammonium nitrate (NH_4NO_3). A small set of NH_3 flux observations recorded at BFRS in 2006 suggests an average NH_3 flux of 7.4 ngN m^{-2} s^{-1} for this location (Fischer and Littlejohn, 2007). If all of this flux is depositional, NH_3 uptake would be competitive with our estimated dry oxidized N deposition flux.

The picture presented in Fig. 12 should be interpreted with care. Relative NO_y mixing ratios and deposition rates can vary widely by location and season. Deposition velocities are still highly uncertain for both APNs and ANs, largely because the mechanisms for uptake or heterogeneous loss are not understood. For example, given that CAFE underestimates PAN exchange velocities during the hot period, it is possible that PAN deposition is faster than represented by the standard resistance parameterization. It is also likely that some deposited species may be re-emitted as NO_2 or nitrous acid (HONO) rather than taken up by vegetation. In an analysis of HONO concentrations measured during BEARPEX-2007, Ren et al. (2010) require an unidentified HONO source of 1.6 ppbv day^{-1}, or 0.02 pptv s^{-1}, to reconcile observations with a steady-state estimate. Heterogeneous HONO production is generally thought to proceed via surface reactions of NO_x (Goodman et al., 1999) and nitrate photolysis (Zhou et al., 2003; He et al., 2006). Assuming this missing source is purely heterogeneous (i.e. production occurs on canopy surfaces) and integrating over the canopy height, we estimate a HONO production flux of 0.2 pptv m s^{-1}, which is ∼67% of the modeled NO_x deposition flux during the hot period. As another example, if the total APN deposition flux during the hot period was treated as an emission of NO_2, NO_x fluxes could increase by as much as 20%. Recent measurements have even suggested that NO_y emitted from canopy surfaces could originate from photolysis of deposited HNO_3 (Raivonen et al., 2006). Future efforts to close the N deposition budget should include direct field

ACPD
10, 21791–21866, 2010

observations of speciated NO_y fluxes and gradients, controlled laboratory experiments on uptake by vegetation and other surfaces (e.g. soil and ground litter), and detailed modeling work.

4 Conclusions

We have used the CAFE model to simulate observations from the BEARPEX-2007 field campaign at Blodgett Forest Research Station in the Sierra Nevada, CA. Our model results highlight a number of interesting features in the extensive BEARPEX-2007 dataset.

1. Comparison of model results with H_2O_2observations suggests that H_2O_2 deposition occurs at the aerodynamic limit, much faster than predicted by standard resistance parameterizations but in agreement with recent direct observations.

2. Modeled O_3 exchange velocities under-predict observations by ∼20% for BEARPEX-2007. This might be partly explained by the lack of a significant contribution from in-canopy chemical loss. Modeled forest-atmosphere exchange will also depend on the magnitude of the cuticular resistance, which is not presently known with sufficient accuracy. Reproducing the chemical flux inferred from previous measurements at BFRS will likely require significant increases in BVOC emissions with high reactivity towards ozone. On a larger scale, such changes carry potential ramifications for quantifying ozone-induced ecosystem stress, BVOC oxidation pathways, and intra-canopy oxidant sources.

3. PAN exchange velocities are under-predicted by 50–60%, which may indicate a reactive surface uptake process not represented by our deposition parameterization. Model-measurement disagreement of PAN fluxes may also stem from an underestimate of the chemical contributions to forest-atmosphere exchange of

ACPD
10, 21791–21866, 2010

APNs. This could be the case if turbulent transport near the ground is less efficient than modeled, as suggested by observed PAN and NO_2 concentration gradients. In-canopy chemical losses enhance modeled above-canopy PAN fluxes by as much as a factor of 2 relative to deposition alone. Chemical production also influences APN fluxes, especially when their formation is closely tied to the oxidation of primary BVOC emissions. Acyl peroxy nitrate fluxes are thus quite sensitive to intra-canopy chemistry and meteorology. In contrast, fluxes of alkyl nitrates and HNO_3 are driven by deposition under our model conditions.

4. HNO_3 dominates model-calculated dry N deposition (which excludes NH_3 and particulate N) during the hot period, though other classes of NO_y become non-negligible ($\sim$28%) during the cool period. Such effects will carry implications for N deposition estimates from routine monitoring networks, which typically only measure wet and dry deposition of NO_3^-/NH_4^+ and HNO_3 (Sparks et al., 2008).

5. The net above-canopy NO_x flux is essentially equal to the soil NO flux but is primarily in the form of NO_2 due to rapid oxidation by O_3, RO_2 and HO_2. Upward NO_2 fluxes cause the net above-canopy NO_y flux to be 30% smaller (less negative) than the gross depositional flux.

It is clear from our results that significant uncertainties still limit our understanding of forest-atmosphere exchange. First, chemical mechanisms fail to reproduce observed HO_x concentrations under high-BVOC conditions. A number of OH-recycling schemes have been postulated to close this gap, but the underlying mechanisms remain unidentified, which will impede the predictive capability of any model aiming to track carbon through the emission and oxidation process. Second, K-theory is a rough approximation to the true structure of turbulent transport within mature canopies, yet it persists as the standard for this type of model. A computationally efficient alternative to K-theory that accurately captures the key features of intra-canopy turbulence would improve confidence in future modeling efforts. Third, a lack of detailed experimental constraints on

ACPD
10, 21791–21866, 2010

the mechanisms and efficiency of depositional processes and on BVOC emission inventories continues to prevent accurate parsing of fluxes into emission, chemistry and deposition. In many instances, parameterizations are tuned so that observed trace gas fluxes are reproduced in models as being purely depositional or as direct emissions from the canopy to the atmosphere. This simplification will bear consequences for accurately modeling ecosystem responses to chemical and climate stresses, such as future changes in temperature and an increasing ozone background.

Acknowledgements. The authors acknowledge support from a National Science Foundation grant ATM-0633897. GMW was partially supported by a US-EPA STAR Fellowship Assistance under Agreement No. FP-91698901. This work has not been formally reviewed by EPA. The views expressed in this work are solely those of the authors; EPA and NSF do not endorse any products or commercial services mentioned. The authors also thank F. Paulot for helpful discussions on isoprene oxidation and S. Fares for his insights on ozone fluxes.

References

Atkinson, R. and Arey, J.: Gas-phase tropospheric chemistry of biogenic volatile organic compounds: a review, Atmos. Environ., 37, S197–S219, 2003.

Baker, B., Guenther, A., Greenberg, J., Goldstein, A., and Fall, R.: Canopy fluxes of 2-methyl-3-buten-2-ol over a ponderosa pine forest by relaxed eddy accumulation: Field data and model comparison, J. Geophys. Res., 104, 26107–26114, 1999.

Bauer, M. R., Hultman, N. E., Panek, J. A., and Goldstein, A. H.: Ozone deposition to a ponderosa pine plantation in the Sierra Nevada Mountains (CA): A comparison of two different climatic years, J. Geophys. Res., 105, 22123–22136, 2000.

Bouvier-Brown, N. C., Goldstein, A. H., Gilman, J. B., Kuster, W. C., and de Gouw, J. A.: In-situ ambient quantification of monoterpenes, sesquiterpenes, and related oxygenated compounds during BEARPEX 2007: implications for gas- and particle-phase chemistry, Atmos. Chem. Phys., 9, 5505-5518, doi:10.5194/acp-9-5505-2009, 2009a.

Bouvier-Brown, N. C., Goldstein, A. H., Worton, D. R., Matross, D. M., Gilman, J. B., Kuster, W. C., Welsh-Bon, D., Warneke, C., de Gouw, J. A., Cahill, T. M., and Holzinger, R.: Methyl

ACPD

10, 21791–21866, 2010

chavicol: characterization of its biogenic emission rate, abundance, and oxidation products in the atmosphere, Atmos. Chem. Phys., 9, 2061–2074, doi:10.5194/acp-9-2061-2009, 2009b.
Bouvier-Brown, N. C., Holzinger, R., Palitzsch, K., and Goldstein, A. H.: Large emissions of sesquiterpenes and methyl chavicol quantified from branch enclosure measurements, Atmos. Environ., 43, 389–401, 2009c.
Butkovskaya, N. I., Pouvesle, N., Kukui, A., and Le Bra, G.: Mechanism of the OH-initiated oxidation of glycolaldehyde over the temperature range 233–296 K, J. Phys. Chem. A, 110, 13492–13499, 2006.
Bytnerowicz, A. and Fenn, M. E.: Nitrogen deposition in California forests: a review, Environ. Pollut., 92, 127–146, 1996.
Cantrell, C. A., Lind, J. A., Shetter, R. E., Calvert, J. G., Goldan, P. D., Kuster, W., Fehsenfeld, F. C., Montzka, S. A., Parrish, D. D., Williams, E. J., Buhr, M. P., Westberg, H. H., Allwine, G., and Martin, R.: Peroxy-Radicals In The Rose Experiment – Measurement And Theory, J. Geophys. Res.-Atmos., 97, 20671–20686, 1992.
Choi, W., Faloona, I. C., Bouvier-Brown, N. C., McKay, M., Goldstein, A. H., Mao, J., Brune, W. H., LaFranchi, B. W., Cohen, R. C., Wolfe, G. M., Thornton, J. A., Sonnenfroh, D. M., and Millet, D. B.: Observations of elevated formaldehyde over a forest canopy suggest missing sources from rapid oxidation of arboreal hydrocarbons, Atmos. Chem. Phys. Discuss., 10, 9839–9893, doi:10.5194/acpd-10-9839-2010, 2010.
Ciccioli, P., Brancaleoni, E., Frattoni, M., Di Palo, V., Valentini, R., Tirone, G., Seufert, G., Bertin, N., Hansen, U., Csiky, O., Lenz, R., and Sharma, M.: Emission of reactive terpene compounds from orange orchards and their removal by within-canopy processes, J. Geophys. Res.-Atmos., 104, 8077–8094, 1999.
Coe, H., Gallagher, M. W., Choularton, T. W., and Dore, C.: Canopy Scale Measurements Of Stomatal And Cuticular O-3 Uptake By Sitka Spruce, Atmos. Environ., 29, 1413–1423, 1995.
Cohen, R. C., Goldstein, A. H., and Thornton, J. A.: The Biosphere Effects on Aerosol and Photochemistry EXperiment (BEARPEX), Atmos. Chem. Phys. Discuss., in preparation, 2010.
Crounse, J. D., McKinney, K. A., Kwan, A. J., and Wennberg, P. O.: Measurement of gas-phase hydroperoxides by chemical ionization mass spectrometry, Anal. Chem., 78, 6726–6732, 2006.
Da Silva, G., Graham, C., and Wang, Z. F.: Unimolecular beta-Hydroxyperoxy Radical Decomposition with OH Recycling in the Photochemical Oxidation of Isoprene, Environ. Sci.

ACPD
10, 21791–21866, 2010

Technol., 44, 250–256, 2010.
Darrall, N. M.: The Effect Of Air-Pollutants On Physiological Processes In Plants, Plant Cell Environ., 12, 1–30, 1989.
Day, D. A., Wooldridge, P. J., and Cohen, R. C.: Observations of the effects of temperature on atmospheric HNO_3, ΣANs, ΣPNs, and NO_x: evidence for a temperature-dependent HO_x source, Atmos. Chem. Phys., 8, 1867–1879, doi:10.5194/acp-8-1867-2008, 2008.
Day, D. A., Farmer, D. K., Goldstein, A. H., Wooldridge, P. J., Minejima, C., and Cohen, R. C.: Observations of NO_x, ΣPNs, ΣANs, and HNO_3 at a Rural Site in the California Sierra Nevada Mountains: summertime diurnal cycles, Atmos. Chem. Phys., 9, 4879–4896, doi:10.5194/acp-9-4879-2009, 2009.
Di Carlo, P., Brune, W. H., Martinez, M., Harder, H., Lesher, R., Ren, X. R., Thornberry, T., Carroll, M. A., Young, V., Shepson, P. B., Riemer, D., Apel, E., and Campbell, C.: Missing OH reactivity in a forest: Evidence for unknown reactive biogenic VOCs, Science, 304, 722–725, 2004.
Dillon, M. B., Lamanna, M. S., Schade, G. W., Goldstein, A., and Cohen, R. C.: Chemical evolution of the Sacramento urban plume: Transport and oxidation, J. Geophys. Res., 107, 4045, doi:10.1029/2001JD000969, 2002.
Dorsey, J. R., Duyzer, J. H., Gallagher, M. W., Coe, H., Pilegaard, K., Weststrate, J. H., Jensen, N. O., and Walton, S.: Oxidized nitrogen and ozone interaction with forests. I: Experimental observations and analysis of exchange with Douglas fir, Q. J. Roy. Meteorol. Soc., 130, 1941–1955, 2004.
Dreyfus, G. B., Schade, G. W., and Goldstein, A. H.: Observational constraints on the contribution of isoprene oxidation to ozone production on the western slope of the Sierra Nevada, California, J. Geophys. Res.-Atmos., 107, 4365–4382, 2002.
Duyzer, J. H., Dorsey, J. R., Gallagher, M. W., Pilegaard, K., and Walton, S.: Oxidized nitrogen and ozone interaction with forests. II: Multi-layer process-oriented modelling results and a sensitivity study for Douglas fir, Q. J. Roy. Meteorol. Soc., 130, 1957–1971, 2004.
Erisman, J. W., Vanpul, A., and Wyers, P.: Parametrization Of Surface-Resistance For The Quantification Of Atmospheric Deposition Of Acidifying Pollutants And Ozone, Atmos. Environ., 28, 2595–2607, 1994.
Erisman, J. W., Draaijers, G. P. J., Steingrover, E., Van Dijk, H., Boxman, A., and de Vries, W.: Assessment of the exposure and loads of acidifying and eutrophying pollutants and ozone, as well as their, harmful influence on the vitality of the trees and the Speulder forest

ACPD
10, 21791–21866, 2010

ecosystem as a whole, Water Air Soil Pollut., 105, 539–571, 1998.
Erisman, J. W., Vermeulen, A., Hensen, A., Flechard, C., Dammgen, U., Fowler, D., Sutton, M., Grunhage, L., and Tuovinen, J. P.: Monitoring and modelling of biosphere/atmosphere exchange of gases and aerosols in Europe, Environ. Pollut., 133, 403–413, 2005.
Faloona, I., Tan, D., Brune, W., Hurst, J., Barket, D., Couch, T. L., Shepson, P., Apel, E., Riemer, D., Thornberry, T., Carroll, M. A., Sillman, S., Keeler, G. J., Sagady, J., Hooper, D., and Paterson, K.: Nighttime observations of anomalously high levels of hydroxyl radicals above a deciduous forest canopy, J. Geophys. Res.-Atmos., 106, 24315–24333, 2001.
Faloona, I. C., Tan, D., Lesher, R. L., Hazen, N. L., Frame, C. L., Simpas, J. B., Harder, H., Martinez, M., Di Carlo, P., Ren, X. R., and Brune, W. H.: A laser-induced fluorescence instrument for detecting tropospheric OH and HO_2: Characteristics and calibration, J. Atmos. Chem., 47, 139–167, 2004.
Fares, S., McKay, M., Holzinger, R., and Goldstein, A. H.: Ozone fluxes in a Pinus ponderosa ecosystem are dominated by non-stomatal processes: Evidence from long-term continuous measurements, Agr. Forest Meteorol., 150, 420–431, 2010.
Farmer, D. K. and Cohen, R. C.: Observations of HNO_3, ΣAN, ΣPN and NO_2 fluxes: evidence for rapid HO_x chemistry within a pine forest canopy, Atmos. Chem. Phys., 8, 3899–3917, doi:10.5194/acp-8-3899-2008, 2008.
Farmer, D. K., Cohen, R. C., Perring, A. E., Wooldridge, P. J., Blake, D., Baker, A., Huey, L. G., Sjostedt, S., Tanner, D., O.Vargas, Gouw, J. d., Warneke, C., Kuster, W., and Murphy, J. G.: NO_y partitioning and the role of alkyl nitrates in air quality in the Mexico City area, in preparation, 2010.
M. L. Fischer and D. Littlejohn: Ammonia at Blodgett Forest, Sierra Nevada, USA, Atmos. Chem. Phys. Discuss., 7, 14139–14169, doi:10.5194/acpd-7-14139-2007, 2007.
Forkel, R., Klemm, O., Graus, M., Rappengluck, B., Stockwell, W. R., Grabmer, W., Held, A., Hansel, A., and Steinbrecher, R.: Trace gas exchange and gas phase chemistry in a Norway spruce forest: A study with a coupled 1-dimensional canopy atmospheric chemistry emission model, Atmos. Environ., 40, S28–S42, 2006.
Fowler, D., Pilegaard, K., Sutton, M. A., Ambus, P., Raivonen, M., Duyzer, J., Simpson, D., Fagerli, H., Fuzzi, S., Schjoerring, J. K., Granier, C., Neftel, A., Isaksen, I. S. A., Laj, P., Maione, M., Monks, P. S., Burkhardt, J., Daemmgen, U., Neirynck, J., Personne, E., Wichink-Kruit, R., Butterbach-Bahl, K., Flechard, C., Tuovinen, J. P., Coyle, M., Gerosa, G., Loubet, B., Altimir, N., Gruenhage, L., Ammann, C., Cieslik, S., Paoletti, E., Mikkelsen, T. N., Ro-

ACPD
10, 21791–21866, 2010

Poulsen, H., Cellier, P., Cape, J. N., Horvath, L., Loreto, F., Niinemets, U., Palmer, P. I., Rinne, J., Misztal, P., Nemitz, E., Nilsson, D., Pryor, S., Gallagher, M. W., Vesala, T., Skiba, U., Brueggemann, N., Zechmeister-Boltenstern, S., Williams, J., O'Dowd, C., Facchini, M. C., de Leeuw, G., Flossman, A., Chaumerliac, N., and Erisman, J. W.: Atmospheric composition change: Ecosystems-Atmosphere interactions, Atmos. Environ., 43, 5193–5267, 2009.

Fuentes, J. D., Hayden, B. P., Garstang, M., Lerdau, M., Fitzjarrald, D., Baldocchi, D. D., Monson, R., Lamb, B., and Geron, C.: New Directions: VOCs and biosphere-atmosphere feedbacks, Atmos. Environ., 35, p. 189, 2001.

Ganzeveld, L., Valverde-Canossa, J., Moortgat, G. K., and Steinbrecher, R.: Evaluation of peroxide exchanges over a coniferous forest un a single-column chemistry-climate model, Atmos. Environ., 40, S68–S80, doi:10.1016/j.atmosenv.2006.01.062, 2006.

Gao, W., Wesely, M. L., and Lee, I. Y.: A numerical study of the effects of air chemistry on fluxes of NO, NO_2, and O_3 near the surface, J. Geophys. Res., 96, 18761–18769, 1991.

Gao, W., Wesely, M. L., and Doskey, P. V.: Numerical modeling of the turbulent diffusion and chemistry of NO_x, O_3, isoprene, and other reactive trace gases in and above a forest canopy, J. Geophys. Res., 98, 18339–18353, 1993.

Goldan, P. D., Kuster, W. C., Williams, E., Murphy, P. C., Fehsenfeld, F. C., and Meagher, J.: Nonmethane hydrocarbon and oxy hydrocarbon measurements during the 2002 New England Air Quality Study, J. Geophys. Res.-Atmos., 109, D21309, doi:10.1029/2003JD004455, 2004.

Goldstein, A. H., Hultman, N. E., Fracheboud, J. M., Bauer, M. R., Panek, J. A., Xu, M., Qi, Y., Guenther, A. B., and Baugh, W.: Effects of climate variability on the carbon dioxide, water, and sensible heat fluxes above a ponderosa pine plantation in the Sierra Nevada (CA), Agr. Forest Meteorol., 101, 113–129, 2000.

Goldstein, A. H., Schade, G. W., and Dreyfus, G.: Whole Ecosystem Measurements of Biogenic Hydrocarbon Emissions, Final Report, State of California Air Resources Board Award No. 98–328, 2001.

Goldstein, A. H., McKay, M., Kurpius, M. R., Schade, G. W., Lee, A., Holzinger, R., and Rasmussen, R. A.: Forest thinning experiment confirms ozone deposition to forest canopy is dominated by reaction with biogenic VOCs, Geophys. Res. Lett., 31, L22106, doi:10.1029/2004GL021259, 2004.

Goldstein, A. H., Koven, C. D., Heald, C. L., and Fung, I. Y.: Biogenic carbon and anthropogenic pollutants combine to form a cooling haze over the southeastern United States, Proceedings

ACPD
10, 21791–21866, 2010

Of The National Academy Of Sciences Of The United States Of America, 106, 8835–8840, 2009.
Goodman, A. L., Underwood, G. M., and Grassian, V. H.: Heterogeneous reaction of NO_2: Characterization of gas-phase and adsorbed products from the reaction, $2NO_2(g) + H_2O(a) -> HONO(g) + HNO(a)$ on hydrated silica particles, J. Phys. Chem. A, 103, 7217–7223, 1999.
Gray, D. W., Lerdau, M. T., and Goldstein, A. H.: Influences of temperature history, water stress, and needle age on methylbutenol emissions, Ecology, 84, 765–776, 2003.
Gray, D. W., Goldstein, A. H., and Lerdau, M. T.: Thermal history regulates methylbutenol basal emission rate in Pinus ponderosa, Plant Cell Environ., 29, 1298–1308, 2006.
Guenther, A., Hewitt, C. N., Erickson, D., Fall, R., Geron, C., Graedel, T., Harley, P., Klinger, L., Lerdau, M. T., McKay, W. A., Pierce, T., Scholes, B., Steinbrecher, R., Tallamraju, R., Taylor, J., and Zimmerman, P.: A global model of natural volatile organic compound emissions, J. Geophys. Res., 100, 8873–8892, 1995.
Hall, B. D. and Claiborn, C. S.: Measurements of the dry deposition of peroxides to a Canadian boreal forest, J. Geophys. Res.-Atmos., 102, 29343–29353, 1997.
Harley, P., Fridd-Stroud, V., Greenberg, J., Guenther, A., and Vasconcellos, P.: Emission of 2-methyl-3-buten-2-ol by pines: A potentially large natural source of reactive carbon to the atmosphere, J. Geophys. Res., 103, 25479–25486, 1998.
He, Y., Zhou, X. L., Hou, J., Gao, H. L., and Bertman, S. B.: Importance of dew in controlling the air-surface exchange of HONO in rural forested environments, Geophys. Res. Lett., 33, L02813, doi:10.1029/2005GL024348, 2006.
Herman, D. J., Halverson, L. J., and Firestone, M. K.: Nitrogen Dynamics in an Annual Grassland: Oak Canopy, Climate, and Microbial Population Effects, Ecol. Appl., 13, 593–604, 2003.
Hofzumahaus, A., Rohrer, F., Lu, K., Bohn, B., Brauers, T., Chang, C.-C., Fuchs, H., Holland, F., Kita, K., Kondo, Y., Li, X., Lou, S., Shao, M., Zeng, L., Wahner, A., and Zhang, Y.: Amplified Trace Gas Removal in the Troposphere, Science, 324, 1702–1704, doi:10.1126/science.1164566, 2009.
Hogg, A., Uddling, J., Ellsworth, D., Carroll, M. A., Pressley, S., Lamb, B., and Vogel, C.: Stomatal and non-stomatal fluxes of ozone to a northern mixed hardwood forest, Tellus B, 59, 514–525, 2007.
Holzinger, R., Lee, A., Paw, K. T., and Goldstein, U. A. H.: Observations of oxidation products above a forest imply biogenic emissions of very reactive compounds, Atmos. Chem. Phys.,

ACPD
10, 21791–21866, 2010

5, 67–75, doi:10.5194/acp-5-67-2005, 2005.
Horii, C. V., Munger, J. W., Wofsy, S. C., Zahniser, M., Nelson, D., and McManus, J. B.: Atmospheric reactive nitrogen concentration and flux budgets at a Northeastern US forest site, Agr. Forest Meteorol., 136, 159–174, 2006.
Horowitz, L. W., Fiore, A. M., Milly, G. P., Cohen, R. C., Perring, A., Wooldridge, P. J., Hess, P. G., Emmons, L. K., and Lamarque, J. F.: Observational constraints on the chemistry of isoprene nitrates over the eastern United States, J. Geophys. Res.-Atmos., 112, D12S08, doi:10.1029/2006JD007747, 2007.
Huisman, A. J., Hottle, J. R., Coens, K. L., DiGangi, J. P., Galloway, M. M., Kammrath, A., and Keutsch, F. N.: Laser-induced phosphorescence for the in situ detection of glyoxal at part per trillion mixing ratios, Anal. Chem., 80, 5884–5891, 2008.
Isaksen, I. S. A., Granier, C., Myhre, G., Berntsen, T. K., Dalsoren, S. B., Gauss, M., Klimont, Z., Benestad, R., Bousquet, P., Collins, W., Cox, T., Eyring, V., Fowler, D., Fuzzi, S., Jockel, P., Laj, P., Lohmann, U., Maione, M., Monks, P., Prevot, A. S. H., Raes, F., Richter, A., Rognerud, B., Schulz, M., Shindell, D., Stevenson, D. S., Storelvmo, T., Wang, W. C., van Weele, M., Wild, M., and Wuebbles, D.: Atmospheric composition change: Climate-Chemistry interactions, Atmos. Environ., 43, 5138–5192, 2009.
Jacobson, M. Z.: Fundamentals of Atmospheric Modeling, Cambridge University Press, New York, 2005.
Jaeglé, L., Steinberger, L., Martin, R. V., and Chance, K.: Global partitioning of NO_x sources using satellite observations: Relative roles of fossil fuel combustion, biomass burning and soil emissions, Faraday Discuss., 130, 407–423, doi:10.1039/b502128f, 2005.
Kurpius, M. R. and Goldstein, A. H.: Gas-phase chemistry dominates O_3 loss to a forest, implying a source of aerosols and hydroxyl radicals to the atmosphere, Geophys. Res. Lett., 30, 1371–1374, doi:10.1029/2002GL016785, 2003.
LaFranchi, B. W., Wolfe, G. M., Thornton, J. A., Harrold, S. A., Browne, E. C., Min, K. E., Wooldridge, P. J., Gilman, J. B., Kuster, W. C., Goldan, P. D., de Gouw, J. A., McKay, M., Goldstein, A. H., Ren, X., Mao, J., and Cohen, R. C.: Closing the peroxy acetyl nitrate budget: observations of acyl peroxy nitrates (PAN, PPN, and MPAN) during BEARPEX 2007, Atmos. Chem. Phys., 9, 7623–7641, doi:10.5194/acp-9-7623-2009, 2009.
Lee, A., Goldstein, A. H., Keywood, M. D., Gao, S., Varutbangkul, V., Bahreini, R., Ng, N. L., Flagan, R. C., and Seinfeld, J. H.: Gas-phase products and secondary aerosol yields from the ozonolysis of ten different terpenes, J. Geophys. Res., 111, 1–18,

ACPD
10, 21791–21866, 2010

doi:10.1029/2005JD006437, 2006a.
Lee, A., Goldstein, A. H., Kroll, J. H., Ng, N. L., Varutbangkul, V., Flagan, R. C., and Seinfeld, J. H.: Gas-phase products and secondary aerosol yields from the photooxidation of 16 different terpenes, J. Geophys. Res., 111, 1–25, doi:10.1029/2006JD007050, 2006b.
Lelieveld, J., Butler, T. M., Crowley, J. N., Dillon, T. J., Fischer, H., Ganzeveld, L., Harder, H., Lawrence, M. G., Martinez, M., Taraborrelli, D., and Williams, J.: Atmospheric oxidation capacity sustained by a tropical forest, Nature, 452, 737–740, doi:10.1038/nature06870, 2008.
Magnani, F., Mencuccini, M., Borghetti, M., Berbigier, P., Berninger, F., Delzon, S., Grelle, A., Hari, P., Jarvis, P. G., Kolari, P., Kowalski, A. S., Lankreijer, H., Law, B. E., Lindroth, A., Loustau, D., Manca, G., Moncrieff, J. B., Rayment, M., Tedeschi, V., Valentini, R., and Grace, J.: The human footprint in the carbon cycle of temperate and boreal forests, Nature, 447, 849–851, 2007.
Makar, P. A., Fuentes, J. D., Wang, D., Staebler, R. M., and Wiebe, H. A.: Chemical processing of biogenic hydrocarbons within and above a temperate deciduous forest, J. Geophys. Res., 104, 3581–3603, 1999.
Mao, J., Ren, X., Chen, Z., Brune, W., LaFranchi, B., Cohen, R., Gilman, J., and deGouw, J.: HO_x chemistry in and above a forest canopy in seasonal transition, in: Eos Trans. AGU, Fall Meet. Suppl., 89(53), Abstract A32C-03, 2008.
Mao, J., Ren, X., Brune, W. H., Olson, J. R., Crawford, J. H., Fried, A., Huey, L. G., Cohen, R. C., Heikes, B., Singh, H. B., Blake, D. R., Sachse, G. W., Diskin, G. S., Hall, S. R., and Shetter, R. E.: Airborne measurement of OH reactivity during INTEX-B, Atmos. Chem. Phys., 9, 163–173, doi:10.5194/acp-9-163-2009, 2009.
Martinez, M., Harder, H., Kovacs, T. A., Simpas, J. B., Bassis, J., Lesher, R., Brune, W. H., Frost, G. J., Williams, E. J., Stroud, C. A., Jobson, B. T., Roberts, J. M., Hall, S. R., Shetter, R. E., Wert, B., Fried, A., Alicke, B., Stutz, J., Young, V. L., White, A. B., and Zamora, R. J.: OH and HO_2 concentrations, sources, and loss rates during the Southern Oxidants Study in Nashville, Tennessee, summer 1999, J. Geophys. Res.-Atmos., 108, D194617, doi:10.1029/2003JD003551, 2003.
Murphy, J. G., Day, D. A., Cleary, P. A., Wooldridge, P. J., and Cohen, R. C.: Observations of the diurnal and seasonal trends in nitrogen oxides in the western Sierra Nevada, Atmos. Chem. Phys., 6, 5321–5338, doi:10.5194/acp-6-5321-2006, 2006.
Paulot, F., Beaver, M. R., St. Clair, J., Spencer, K. M., Crounse, J., and Wennberg, P. O.:

ACPD
10, 21791–21866, 2010

Exchange of hydrogen peroxide and nitric acid over a ponerosa forest measured by eddy covariance, in: Eos Trans. AGU, Fall Meet. Suppl., 90(52), Abstract A41D-0133, 2009a.
Paulot, F., Crounse, J. D., Kjaergaard, H. G., Kroll, J. H., Seinfeld, J. H., and Wennberg, P. O.: Isoprene photooxidation: new insights into the production of acids and organic nitrates, Atmos. Chem. Phys., 9, 1479–1501, doi:10.5194/acp-9-1479-2009, 2009.
Paulot, F., Crounse, J. D., Kjaergaard, H. G., Kurten, A., St Clair, J. M., Seinfeld, J. H., and Wennberg, P. O.: Unexpected Epoxide Formation in the Gas-Phase Photooxidation of Isoprene, Science, 325, 730–733, 2009c.
Peeters, J., Nguyen, T. L., and Vereecken, L.: HOx radical regeneration in the oxidation of isoprene, Phys. Chem. Phys. Chem., 11, 5935–5939, 2009.
Pérez, I. M., LaFranchi, B. W., and Cohen, R. C.: Nitrogen oxide chemistry in an urban plume: investigation of the chemistry of peroxy and multifunctional organic nitrates with a Lagrangian model, Atmos. Chem. Phys. Discuss., 9, 27099–27165, doi:10.5194/acpd-9-27099-2009, 2009.
Perring, A. E., Bertram, T. H., Wooldridge, P. J., Fried, A., Heikes, B. G., Dibb, J., Crounse, J. D., Wennberg, P. O., Blake, N. J., Blake, D. R., Brune, W. H., Singh, H. B., and Cohen, R. C.: Airborne observations of total $RONO_2$: new constraints on the yield and lifetime of isoprene nitrates, Atmos. Chem. Phys., 9, 1451–1463, doi:10.5194/acp-9-1451-2009, 2009a.
Perring, A. E., Wisthaler, A., Graus, M., Wooldridge, P. J., Lockwood, A. L., Mielke, L. H., Shepson, P. B., Hansel, A., and Cohen, R. C.: A product study of the isoprene + NO_3 reaction, Atmos. Chem. Phys., 9, 4945–4956, doi:10.5194/acp-9-4945-2009, 2009b.
Pryor, S. C. and Klemm, O.: Experimentally derived estimates of nitric acid dry deposition velocity and viscous sub-layer resistance at a conifer forest, Atmos. Environ., 38, 2769–2777, 2004.
Qi, B., Takami, A., and Hatakeyama, S.: Peroxy radical concentrations measured at a forest canopy in Nikko, Japan, in summer 2002, J. Atmos. Chem., 52, 63–79, 2005.
Raivonen, M., Bonn, B., Sanz, M. J., Vesala, T., Kulmala, M., and Hari, P.: UV-induced NO_y emissions from Scots pine: Could they originate from photolysis of deposited HNO_3?, Atmos. Environ., 40, 6201–6213, 2006.
Raupach, M. R.: A practical Lagrangian method for relating scalar concentrations to source distributions in vegetation canopies, Q. J. Roy. Meteorol. Soc., 115, 609–632, 1989.
Ren, X., Gao, H., Zhou, X., Crounse, J. D., Wennberg, P. O., Browne, E. C., LaFranchi, B. W., Cohen, R. C., McKay, M., Goldstein, A. H., and Mao, J.: Measurement of atmospheric

ACPD
10, 21791–21866, 2010

nitrous acid at Blodgett Forest during BEARPEX2007, Atmos. Chem. Phys. Discuss., 10, 7383–7419, doi:10.5194/acpd-10-7383-2010, 2010.

Ren, X. R., Olson, J. R., Crawford, J. H., Brune, W. H., Mao, J. Q., Long, R. B., Chen, Z., Chen, G., Avery, M. A., Sachse, G. W., Barrick, J. D., Diskin, G. S., Huey, L. G., Fried, A., Cohen, R. C., Heikes, B., Wennberg, P. O., Singh, H. B., Blake, D. R., and Shetter, R. E.: HO_x chemistry during INTEX-A 2004: Observation, model calculation, and comparison with previous studies, J. Geophys. Res.-Atmos., 113, D05310, doi:10.1029/2007JD009166, 2008.

Rollins, A. W., Kiendler-Scharr, A., Fry, J. L., Brauers, T., Brown, S. S., Dorn, H.-P., Dubé, W. P., Fuchs, H., Mensah, A., Mentel, T. F., Rohrer, F., Tillmann, R., Wegener, R., Wooldridge, P. J., and Cohen, R. C.: Isoprene oxidation by nitrate radical: alkyl nitrate and secondary organic aerosol yields, Atmos. Chem. Phys., 9, 6685–6703, doi:10.5194/acp-9-6685-2009, 2009.

Rondon, A., Johansson, C., and Granat, L.: Dry Deposition Of Nitrogen-Dioxide And Ozone To Coniferous Forests, J. Geophys. Res.-Atmos., 98, 5159–5172, 1993.

Rummel, U., Ammann, C., Kirkman, G. A., Moura, M. A. L., Foken, T., Andreae, M. O., and Meixner, F. X.: Seasonal variation of ozone deposition to a tropical rain forest in southwest Amazonia, Atmos. Chem. Phys., 7, 5415–5435, doi:10.5194/acp-7-5415-2007, 2007.

Schade, G. W., Goldstein, A. H., Gray, D. W., and Lerdau, M. T.: Canopy and leaf level 2-methyl-3-buten-2-ol fluxes from a ponderosa pine plantation, Atmos. Environ., 34, 3535–3544, 2000.

Seinfeld, J. H. and Pandis, S. N.: Atmospheric Chemistry and Physics, 2nd ed., John Wiley and Sons, Inc., Hoboken, NJ, 2006.

Sievering, H., Kelly, T., McConville, G., Seibold, C., and Turnipseed, A.: Nitric acid dry deposition to conifer forests: Niwot Ridge spruce-fir-pine study, Atmos. Environ., 35, 3851–3859, 2001.

Sitch, S., Cox, P. M., Collins, W. J., and Huntingford, C.: Indirect radiative forcing of climate change through ozone effects on the land-carbon sink, Nature, 448, 791–794, 2007.

Sparks, J. P., Walker, J., Turnipseed, A., and Guenther, A.: Dry nitrogen deposition estimates over a forest experiencing free air CO_2 enrichment, Glob. Change Biol., 14, 768–781, 2008.

Stavrakou, T., Peeters, J., and Müller, J.-F.: Improved global modelling of HO_x recycling in isoprene oxidation: evaluation against the GABRIEL and INTEX-A aircraft campaign measurements, Atmos. Chem. Phys. Discuss., 10, 16551–16588, doi:10.5194/acpd-10-16551-2010, 2010.

ACPD
10, 21791–21866, 2010

Steiner, A. L., Tonse, S., Cohen, R. C., Goldstein, A. H., and Harley, R. A.: Influence of future climate and emissions on regional air quality in California, J. Geophys. Res.-Atmos., 111, D18303, doi:10.1029/2005JD006935, 2006.

Steiner, A. L., Tonse, S., Cohen, R. C., Goldstein, A. H., and Harley, R. A.: Biogenic 2-methyl-3-buten-2-ol increases regional ozone and HO_x sources, Geophys. Res. Lett., 34, L15806, doi:10.1029/2007GL030802, 2007.

Stroud, C., Makar, P., Karl, T., Guenther, A., Geron, C., Turnipseed, A. A., Nemitz, E., Baker, B., Potosnak, M., and Fuentes, J. D.: Role of canopy-scale photochemistry in modifying biogenic-atmosphere exchange of reactive terpenoid species: Results from the CELTIC field study, J. Geophys. Res., 110, doi:10.1029/2005JD005775, 2005.

Tan, D., Faloona, I., Simpas, J. B., Brune, W., Shepson, P. B., Couch, T. L., Sumner, A. L., Carroll, M. A., Thornberry, T., Apel, E., Riemer, D., and Stockwell, W.: HO_x budgets in a deciduous forest: Results from the PROPHET summer 1998 campaign, J. Geophys. Res.-Atmos., 106, 24407–24427, 2001.

Thomas, R. Q., Canham, C. D., Weathers, K. C., and Goodale, C. L.: Increased tree carbon storage in response to nitrogen deposition in the US, Nature Geosci., 3, 13–17, doi:10.1038/ngeo721, 2010.

Thornton, J. A., Wooldridge, P. J., Cohen, R. C., Martinez, M., Harder, H., Brune, W. H., Williams, E. J., Roberts, J. M., Fehsenfeld, F. C., Hall, S. R., Shetter, R. E., Wert, B. P., and Fried, A.: Ozone production rates as a function of NO_x abundances and HO_x production rates in the Nashville urban plume, J. Geophys. Res., 107, 4146–4163, doi:10.1029/2001JD000932, 2002.

Turnipseed, A. A., Huey, L. G., Nemitz, E., Stickel, R., Higgs, J., Tanner, D. J., Slusher, D. L., Sparks, J. P., Flocke, F., and Guenther, A.: Eddy covariance fluxes of peroxyacetyl nitrates (PANs) and NO_y to a coniferous forest, J. Geophys. Res., 111, D09304, doi:10.1029/2005JD006631, 2006.

Walton, S., Gallagher, M. W., and Duyzer, J. H.: Use of a detailed model to study the exchange of NO_x and O-3 above and below a deciduous canopy, Atmos. Environ., 31, 2915–2931, 1997.

Wesely, M. L.: Parameterization of surface resistances to gaseous dry deposition in regional-scale numerical models, Atmos. Environ., 23, 1293–1304, 1989.

Wesely, M. L. and Hicks, B. B.: A review of the current status of knowledge on dry deposition, Atmos. Environ., 34, 2261–2282, 2000.

ACPD

10, 21791–21866, 2010

Williams, E. J., Guenther, A., and Fehsenfeld, F. C.: An inventory of nitric oxide emissions from soils in the united states, J. Geophys. Res., 97, 7511–7519, 1992.

Wolfe, G. M., Thornton, J. A., Yatavelli, R. L. N., McKay, M., Goldstein, A. H., LaFranchi, B., Min, K.-E., and Cohen, R. C.: Eddy covariance fluxes of acyl peroxy nitrates (PAN, PPN and MPAN) above a Ponderosa pine forest, Atmos. Chem. Phys., 9, 615–634, doi:10.5194/acp-9-615-2009, 2009.

Wolfe, G. M. and Thornton, J. A.: The Chemistry of Atmosphere-Forest Exchange (CAFE) Model – Part 1: Model Description and Characterization, Atmos. Chem. Phys. Discuss., Atmos. Chem. Phys. Discuss., 10, 21721-21790, doi:10.5194/acpd-10-21721-2010, 2010.

Wooldridge, P. J., Perring, A. E., Bertram, T. H., Flocke, F. M., Roberts, J. M., Singh, H. B., Huey, L. G., Thornton, J. A., Wolfe, G. M., Murphy, J. G., Fry, J. L., Rollins, A. W., LaFranchi, B. W., and Cohen, R. C.: Total Peroxy Nitrates (ΣPNs) in the atmosphere: the Thermal Dissociation-Laser Induced Fluorescence (TD-LIF) technique and comparisons to speciated PAN measurements, Atmos. Meas. Tech., 3, 593–607, doi:10.5194/amt-3-593-2010, 2010.

Yienger, J. J. and Levy, H.: Empirical-Model Of Global Soil-Biogenic NO_x Emissions, J. Geophys. Res.-Atmos., 100, 11447–11464, 1995.

Zhang, L., Brook, J. R., and Vet, R.: A revised parameterization for gaseous dry deposition in air-quality models, Atmos. Chem. Phys., 3, 2067–2082, doi:10.5194/acp-3-2067-2003, 2003.

Zhang, L. M., Moran, M. D., Makar, P. A., Brook, J. R., and Gong, S. L.: Modelling gaseous dry deposition in AURAMS: a unified regional air-quality modelling system, Atmos. Environ., 36, 537–560, 2002.

Zhou, X. L., Gao, H. L., He, Y., Huang, G., Bertman, S. B., Civerolo, K., and Schwab, J.: Nitric acid photolysis on surfaces in low-NO_x environments: Significant atmospheric implications, Geophys. Res. Lett., 30(23), 2217, doi:10.1029/2003GL018620, 2003.

ACPD
10, 21791–21866, 2010

Table 1. Model parameters.

Parameter	Symbol	Value	Units
Overstory height	h	10	m
Understory height	h_{us}	2	m
Atmospheric boundary layer height	h_{ABL}	800	m
Overstory leaf area index	LAI_{os}	3.2	$m^2\,m^{-2}$
Understory leaf area index	LAI_{us}	1.9	$m^2\,m^{-2}$
Overstory dry leaf mass	d_{os}	219	$g\,m^{-2}$
Understory dry leaf mass	d_{us}	377	$g\,m^{-2}$
Radiation extinction coefficient	k_{rad}	0.4	
Diffusion timescale ratio	τ/T_L	4	
NO basal emission rate	E^b_{NO}	3	$ngN\,m^{-2}\,s^{-1}$
Integration interval	Δt	2	s
Chemistry time step		0.05	s
Diffusion time step		0.05	s
Total integration time		7200	s

ACPD
10, 21791–21866, 2010

Table 2. Meteorological observations.

Parameter	Symbol	Hot	Cool	Units
Air Temperature[a]	T	30.5–28.4	19.8–17.5	°C
Surface pressure[b]	P	870	868	mbar
Actinic flux[b]	RAD	674	618	$W\,m^{-2}$
Photosynthetically Active Radiation[b]	PAR	1758	1595	$umol\,m^{-2}\,s^{-1}$ [d]
Water vapor concentration[b]	H_2O	10.8	10.3	$mmol\,mol^{-1}$
Vapor pressure deficit[b]	VPD	2.91	1.10	kPa
Friction velocity[b]	u^*	0.63	0.68	$m\,s^{-1}$
Solar Zenith Angle[c]	SZA	30.4	36.3	degrees

[a] Range of measurements from 3.0–12.5 m.
[b] Measured at 12.5 m.
[c] From TUV model.
[d] Divide by 2.92 to convert to $W\,m^{-2}$.

ACPD
10, 21791–21866, 2010

Table 3. Enhanced OH-recycling reactions. All reactions have a rate constant of 4.5×10^{-11} cm^3 $molec^{-1}$ s^{-1}. α is set to 2.6.

Reaction
$MBOAO_2 + HO_2 \rightarrow \alpha OH + HOCH_2CHO + CH_3COCH_3 + HO_2$
$MBOBO_2 + HO_2 \rightarrow \alpha OH + IBUTALOH + HCHO + HO_2$
$ISOPAO_2 + HO_2 \rightarrow \alpha OH + HC4CCHO + HO_2$
$ISOPBO_2 + HO_2 \rightarrow \alpha OH + 0.25\,(MVKOH + CH_3O_2) + 0.75\,(MVK + HCHO + HO_2)$
$ISOPCO_2 + HO_2 \rightarrow \alpha OH + HC4ACHO + HO_2$
$ISOPDO_2 + HO_2 \rightarrow \alpha OH + MACR + HCHO + HO_2$

ACPD
10, 21791–21866, 2010

Table 4. Initial/advection concentrations in ppbv. Species not listed have initial/advection concentrations set to 0.

Species	Mixing Ratio/ppbv Hot	Mixing Ratio/ppbv Cool	Species	Mixing Ratio/ppbv Hot	Mixing Ratio/ppbv Cool
OH	3×10^{-4}	1×10^{-4}	**Aldehydes**		
HO_2	0.03	0.02	HCHO	3	1
CO	97	116	CH_3CHO	0.4	0.5
O_3	53	45	C_2H_5CHO	0.13	0.13
			MACR	0.1	0.3
			GLYOX	0.03	0.03
NO_y					
NO	0.1	0.1			
NO_2	0.5	0.8	**Hydrocarbons**		
HNO_3	0.82	0.25	CH_4	1600	1600
PAN	0	0.26	isoprene	4	0.2
PPN	0	0.02	C_3H_6	0.1	0.1
MPAN	0	0.03			
$MBOANO_3$	0.05	0.04	**Ketones**		
$MBOBNO_3$	0.04	0.03	CH_3COCH_3	1.5	1.7
$ISOPANO_3$	0.03	0.02	MVK	1.6	0.3
$ISOPBNO_3$	0.04	0.03	ACETOL	0	0.02
$ISOPCNO_3$	0.03	0.02			
$ISOPDNO_3$	0.03	0.02	**Organic Acids**		
			CH_3CO_2H	6	3
Peroxides			HCOOH	5.5	3.5
H_2O_2	0.9	0.8	CH_3CO_3H	0.24	0.16
Alcohols			**Other**		
MBO	1	0.15	MCHAV	0	0
CH_3OH	5.6	4.6	MT (all)	0	0
C_2H_5OH	1.8	1.6	SQT (all)	0	0
IPROPOL	0.09	0.09	IEPOX	0	0

ACPD
10, 21791–21866, 2010

Table 5. BEARPEX-2007 chemical observations. Statistics are calculated from a merged, 30-min averaged dataset. Concentrations and standard deviations are in ppbv unless otherwise specified.

Species	Height[c]	Hot Period[a]			Cool Period[b]			Ref.[g]
	m	$\bar{C}$[d]	σ_C^e	N[f]	$\bar{C}$[d]	σ_C^e	N[f]	
OH (10^6 molec cm^{-3})	9.4	6.8	0.5	4	4.0	1.2	7	i
	15	8.0	2.7	8				
HO_2	9.4	0.029	0.003	4	0.021	0.004	7	i
	15	0.033	0.005	8				
CO	12.5	97	14	21	116	10	18	ii
O_3	1.2	49.6	11.0	7	44.0	6.6	6	iii
	4.9	51.3	11.4	7	45.5	6.6	6	
	8.75	51.6	11.3	7	45.3	6.0	6	
	12.5	50.8	11.6	7	45.5	5.5	6	
τ_{OH}^{-1} (s^{-1})	9.9	12.4	2.0	17	6.8	1.2	12	iv
NO_y								
NO_2	4.9	0.273	0.135	3	0.314	0.074	11	v
	9	0.139	0.065	4	0.368	0.115	12	
	12.7	0.050	0.022	3	0.346	0.091	13	
ΣPN[h]	4.9				0.458	0.101	9	v
	9	0.185	0.104	3	0.430	0.099	11	
	12.7	0.295	0.177	3	0.413	0.097	12	
ΣAN[i]	4.9	0.142	0.035	2	0.130	0.072	11	v
	9	0.147	0.146	2	0.119	0.066	11	
	12.7				0.096	0.074	10	
PAN	1.5	0.130	0.078	14	0.458	0.171	12	vi
	5	0.152	0.070	14	0.471	0.154	12	
	17.8	0.159	0.079	7	0.449	0.129	6	
PPN	1.5	0.006	0.004	14	0.039	0.014	12	vi
	5	0.009	0.005	14	0.041	0.014	12	
	17.8	0.009	0.005	7	0.039	0.011	6	

ACPD
10, 21791–21866, 2010

Table 5. Continued.

Species	Height[c]	Hot Period[a]			Cool Period[b]			Ref.[g]
	m	$\bar{C}$[d]	σ_C^e	N[f]	$\bar{C}$[d]	σ_C^e	N[f]	
MPAN	1.5	0.031	0.012	14	0.029	0.009	12	vi
	5	0.031	0.013	14	0.034	0.014	12	
	17.8	0.020	0.011	7	0.030	0.011	6	
HNO_3	16.8	0.555	0.190	16	0.273	0.004	3	vii
HONO	16.8	0.022	0.014	9	0.046	0.007	2	vii
Alkenes								
isoprene	6.4	1.645	0.676	20	0.211	0.071	15	viii
Organic Acids								
CH_3CO_2H	16.8	4.494	2.398	16	2.078	0.149	3	vii
HCOOH	16.8	4.099	2.530	13	2.396	0.028	3	vii
CH_3CO_3H	16.8	0.289	0.087	12	0.138	0.012	3	vii
Alcohols								
MBO	6.4	3.182	1.092	20	0.623	0.261	15	viii
CH_3OH	6.4	5.637	1.683	20	4.644	1.083	15	viii
C_2H_5OH	6.4	1.560	0.519	20	1.400	0.389	15	viii
IPROPOL	6.4	0.080	0.035	20	0.074	0.016	15	viii
Aldehydes								
MACR	6.4	0.404	0.189	20	0.120	0.036	15	viii
CH_3CHO	6.4	0.549	0.185	20	0.426	0.100	15	viii
C_2H_5CHO	6.4	0.066	0.015	20	0.061	0.014	15	viii
GLYOX	3, 12	0.077	0.022	21	0.037	0.002	9	ix
HCHO	11.8				12.5	4.0	9	xi
Ketones								
MVK	6.4	1.448	0.664	20	0.140	0.065	15	viii
CH_3COCH_3	6.4	2.446	0.843	20	1.948	0.371	15	viii
ACETOL	16.8	0.243	0.130	12	0.165	0.025	15	vii
NOPINONE	1.5, 9.2	0.007	0.005	5	0.005	0.004	4	x

ACPD
10, 21791–21866, 2010

Table 5. Continued.

Species	Height[c] m	Hot Period[a] $\bar{C}$[d]	σ_C[e]	N[f]	Cool Period[b] $\bar{C}$[d]	σ_C[e]	N[f]	Ref.[g]
Peroxides								
H_2O_2	16.8	0.884	0.191	16	0.634	0.054	3	vii
ISOPOOH + IEPOX	16.8	0.247	0.147	12	0.055	0.010	3	vii
Terpenoids								
α−pinene	1.5, 9.2	0.079	0.008	5	0.024	0.003	3	x
	6.4	0.047	0.011	20	0.013	0.003	15	viii
β−pinene	1.5, 9.2	0.232	0.005	5	0.074	0.007	4	x
	6.4	0.152	0.042	20	0.044	0.012	15	viii
limonene	1.5, 9.2	0.061	0.006	5	0.012	0.008	4	x
	6.4	0.011	0.003	20	0.003	0.001	15	viii
3-carene	1.5, 9.2	0.148	0.021	5	0.040	0.004	3	x
myrcene	1.5, 9.2	0.009	0.001	5	0.003	0.000	4	x
camphene	1.5, 9.2	0.004	0.002	5	bdl	bdl	4	x
terpinolene	1.5, 9.2	0.004	0.002	5	bdl	bdl	4	x
α−terpinene	1.5, 9.2	bdl[j]	bdl	5	bdl	bdl	4	x
γ−terpinene	1.5, 9.2	0.001	0.001	5	bdl	bdl	4	x
methyl chavicol	1.5, 9.2	0.079	0.013	5	0.037	0.006	4	x
α−bergamotene	1.5, 9.2	0.034	0.002	5	0.003	0.001	4	x
unspeciated SQT	1.5, 9.2	0.022	0.007	5	0.003	0.001	4	x

[a] Averages from 28 August–3 September, 11:30–12:30 PST.
[b] Averages from 13–18 September, 11:30–12:30 PST.
[c] Comma-separated values denote different measuring heights for hot and cold periods.
[d] Mean concentration.
[e] Standard deviation.
[f] Number of points in average.
[g] Measurement references: (i) Faloona et al. (2004). (ii) Goldstein et al. (2000). (iii) Bauer et al. (2000). (iv) Mao et al. (2009). (v) Farmer et al. (2010). (vi) Wolfe et al. (2009). (vii) Crounse et al. (2006). (viii) Goldan et al. (2004). (ix) Huisman et al. (2008). (x) Bouvier-Brown et al. (2009a). (xi) Choi et al. (2010).
[h] Sum peroxy nitrates.
[i] Sum alkyl nitrates.
[j] bdl = below detection limit.

ACPD
10, 21791–21866, 2010

Table 6. BVOC and peroxides.

Species	Height m	Concentrations/pptv Model[a]	Meas[b]	% Difference[c]
Hot				
MBO	6.4	3134	3182 ± 1092	−2
isoprene	6.4	1618	1645 ± 676	−2
MCHAV	1.5	81	79 ± 13	+3
MT	1.5	501	538 ± 46	−7
SQT	1.5	55	56 ± 9	−1
MTOX	10	101		
SQTOX	10	41		
ISOPOOH + IEPOX[d]	16.8	304	247 ± 147	+23
H_2O_2	16.8	891 (1324[e])	884 ± 191	−1
Cool				
MBO	6.4	671	623 ± 261	+8
isoprene	6.4	259	211 ± 71	+23
MCHAV	9.2	11	37 ± 6	−70
MT	9.2	82	213 ± 38	−61
SQT	9.2	15	6 ± 2	+152
MTOX	10	23		
SQTOX	10	18		
ISOPOOH[d]	16.8	20	55 ± 10	−64
H_2O_2	16.8	524 (769[e])	634 ± 4	−17

[a] Model results in layer closest to measurement height.
[b] Mean ± standard deviation.
[c] Calculated as 100 · (Model–Meas)/Meas.
[d] Sum of four isomers (ISOPAOOH + ISOPBOOH + ISOPCOOH + ISOPDOOH) and the epoxide IEPOX.
[e] Model results with Henry's law constant for H_2O_2 deposition set to 1×10^5 M atm^{-1}.

ACPD
10, 21791–21866, 2010

Table 7. Contributions to modeled ozone and PAN exchange velocities ($cm\,s^{-1}$). For these species, the "surface" contribution is equivalent to total deposition.

Process	Ozone[a]		PAN[a]	
	Hot	Cool	Hot	Cool
Stomatal dep.	−0.13	−0.23	−0.08	−0.14
Non-stomatal dep.	−0.12	−0.12	−0.01	−0.01
Ground dep.	−0.05	−0.05	−0.03	−0.03
Surface	−0.30	−0.40	−0.12	−0.18
Chemical	0.02	0.01	−0.10	−0.08
Surf + Chem	−0.28	−0.39	−0.22	−0.26
Measured[b]	−0.37 ± 0.12	−0.49 ± 0.11	−0.63 ± 0.25	−0.49 ± 0.27
% Difference[c]	−24	−20	−65	−47

[a] Model results in layer closest to measurement height (12.5 m for O_3, 17.8 m for PAN).
[b] Mean ± standard deviation.
[c] Calculated as 100 · (Model–Meas)/Meas, where Model = Surf + Chem.

ACPD
10, 21791–21866, 2010

Table 8. NO_y speciation.

Species	Height	Concentrations/pptv		% of Σ NO_y	
	m	Model[a]	Meas[b]	Model	Meas
Hot					
NO[c]	9	27		2	
NO_2	9	159	139 ± 65	12	14
Σ PN	9	479	185 ± 104	36	18
ΣAN	9	108	147 ± 146	8	14
HNO_3	16.8	571	555 ± 190	43	54
ΣNO_y[d]		1344	1028 ± 505		
Cool					
NO[c]	9	124		9	
NO_2	9	351	368 ± 115	24	30
ΣPN	9	605	430 ± 99	42	38
ΣAN	9	81	119 ± 66	6	10
HNO_3	16.8	277	273 ± 4	19	22
ΣNO_y[d]		1437	1234 ± 284		

[a] Model results in layer closest to measurement height.
[b] Mean ± standard deviation.
[c] Not measured.
[d] $\Sigma NO_y = NO + NO_2 + \Sigma PN + \Sigma AN + HNO_3$.

ACPD
10, 21791–21866, 2010

Table 9. APN exchange velocities. All measurements are from 17.8 m; model results are from the layer closest to this height.

Species	Height m	V_{ex}/cm s^{-1} Model[a]	Meas[a]
Hot			
PAN	17.8	−0.22	−0.63 ± 0.25
PPN	17.8	−0.20	−3.3 ± 1.0
MPAN	17.8	−0.13	−1.2 ± 1.2
Cool			
PAN	17.8	−0.26	−0.49 ± 0.27
PPN	17.8	−0.26	−0.2 ± 0.54
MPAN	17.8	−0.17	0.26 ± 0.77

[a] Mean ± standard deviation.

ACPD
10, 21791–21866, 2010

Appendix A
Chemical nomenclature

Table A1. MCM nomenclature and molecular structures (http://mcm.leeds.ac.uk/MCM/).

MCM Abbreviation	Structure
MBO	$CH_2CHC(CH_3)_2OH$
C5H8 (isoprene)	$CH_2C(CH_3)CHCH_2$
MVK	$CH_2CHC(O)CH_3$
MACR	$CH_2C(CH_3)CHO$
IBUTALOH	$HOC(CH_3)_2CHO$
HOCH2CHO	$HOCH_2CHO$
MVKOH	$CH_2CHC(O)CH_2OH$
ROOH	
ISOPAOOH	$HOCH_2C(CH_3)CHCH_2O_2H$
ISOPBOOH	$CH_2CHC(CH_2OH)(CH_3)O_2H$
ISOPCOOH	$HOCH_2CHC(CH_3)CH_2O_2H$
ISOPDOOH	$CH_2C(CH_3)CH(CH_2OH)O_2H$
MBOAOOH	$HOC(CH_3)_2CH(CH_2OH)O_2H$
MBOBOOH	$HOC(CH_3)_2CH(OH)CH_2O_2H$
ISOPBO2	$CH_2CHC(CH_2OH)(CH_3)O_2$
APNs	
PAN	$CH_3C(O)O_2NO_2$
PPN	$CH_3CH_2C(O)O_2NO_2$
MPAN	$CH_2C(CH_3)C(O)O_2NO_2$
PHAN	$HOCH_2C(O)O_2NO_2$
C4PAN5	$HOC(CH_3)_2C(O)O_2NO_2$
C4PAN6	$CH_3C(O)CH(OH)C(O)O_2NO_2$
C5PAN17	$HOCH_2CH(CH_3)CHC(O)O_2NO_2$
C5PAN19	$HOCH_2CHC(CH_3)C(O)O_2NO_2$
CH3CO3	$CH_3C(O)O_2$
C2H5CO3	$CH_3CH_2C(O)O_2$
MACO3	$CH_2C(CH_3)C(O)O_2$
ANs	
MBOANO3	$HOC(CH_3)_2CH(CH_2OH)ONO_2$
MBOBNO3	$HOC(CH_3)_2CH(OH)CH_2ONO_2$
ISOPANO3	$HOCH_2C(CH_3)CHCH_2ONO_2$
ISOPBNO3	$CH_2CHC(CH_2OH)(CH_3)ONO_2$
ISOPCNO3	$HOCH_2CHC(CH_3)CH_2ONO_2$
ISOPDNO3	$CH_2C(CH_3)CH(CH_2OH)ONO_2$

ACPD
10, 21791–21866, 2010

Appendix B
Model-Measurement Comparison

Table B1. Model-measurement inter-comparison for selected observations. Values are in ppbv unless otherwise specified.

Species	Height[a]	Hot Period			Cool Period		
	m	Model	Meas[b]	% Diff.[c]	Model	Meas	% Diff.
O_3	12.5	51.5	50.8	1.4	45.3	45.5	−0.3
CO	12.5	97	97	0.4	113	116	−3.0
OH[d]	9.4	6.8	6.8	0	3.7	4.0	−7.5
HO_2	9.4	0.034	0.029	16.7	0.017	0.021	−16.9
NO_y							
NO_2	9	0.159	0.139	14.4	0.351	0.368	−4.7
PAN	17.8	0.256	0.159	61.0	0.461	0.449	2.8
PPN	17.8	0.010	0.009	12.2	0.041	0.039	4.7
MPAN	17.8	0.036	0.031	14.8	0.036	0.03	20.2
ΣPN	9	0.479	0.185	158.8	0.605	0.43	40.7
ΣAN	9	0.108	0.142	−24.1	0.081	0.119	−31.9
HNO_3	16.8	0.571	0.555	2.9	0.277	0.273	1.3
HONO	16.8	0.001	0.022	−97.4	0.004	0.046	−92.2
Alkenes							
isoprene	6.4	1.619	1.645	−1.6	0.259	0.211	22.8
Organic Acids							
CH_3CO_2H	16.8	4.542	4.494	1.1	2.179	2.078	4.9
HCOOH	16.8	4.046	4.099	−1.3	2.530	2.396	5.6
CH_3CO_3H	16.8	0.298	0.289	3.0	0.140	0.138	1.5
Alcohols							
MBO	6.4	3.134	3.182	−1.5	0.671	0.623	7.8
CH_3OH	6.4	5.332	5.637	−5.4	4.310	4.644	−7.2
C_2H_5OH	6.4	1.575	1.56	1.0	1.378	1.4	−1.6
IPROPOL	6.4	0.077	0.08	−3.8	0.073	0.074	−1.7
Aldehydes							
MACR	6.4	0.393	0.404	−2.8	0.120	0.12	−0.2
CH_3CHO	6.4	0.402	0.549	−26.8	0.410	0.426	−3.8
C_2H_5CHO	6.4	0.065	0.066	−0.8	0.061	0.061	−0.7
GLYOX	3.12	0.079	0.077	2.0	0.029	0.037	−20.7
HCHO	11.8	4.263			1.375	12.5	−89.0

ACPD
10, 21791–21866, 2010

Appendix B
Model-Measurement Comparison

Table B1. Continued.

Species	Height[a]	Hot Period			Cool Period		
	m	Model	Meas[b]	% Diff.[c]	Model	Meas	% Diff.
Ketones							
MVK	6.4	1.491	1.448	2.9	0.195	0.14	39.2
CH_3COCH_3	6.4	2.575	2.446	5.3	1.872	1.948	−3.9
ACETOL	16.8	0.297	0.243	22.2	0.168	0.165	2.0
NOPINONE	1.5, 9.2	0.011	0.007	52.1	0.005	0.005	1.0
Peroxides							
H_2O_2	16.8	0.891	0.884	0.8	0.524	0.634	−17.4
ISOPOOH + IEPOX	16.8	0.304	0.247	−23	0.020	0.055	−64
Terpenoids							
α−pinene	1.5, 9.2	0.062	0.079	−21.4	0.014	0.024	−40.6
β−pinene	1.5, 9.2	0.119	0.232	−48.5	0.023	0.074	−69.1
limonene	1.5, 9.2	0.033	0.061	−45.9	0.009	0.012	−21.9
3-carene	1.5, 9.2	0.056	0.148	−62.0	0.014	0.04	−66.1
myrcene	1.5, 9.2	0.027	0.009	200.1	0.006	0.003	111.4
camphene	1.5, 9.2	0.039	0.004	870.0	0.011	bdl	
terpinolene	1.5, 9.2	0.005	0.004	14.2	0.001	bdl	
α−terpinene	1.5, 9.2	0.008	bdl[e]		0.002	bdl	
γ−terpinene	1.5, 9.2	0.005	0.001	449.4	0.002	bdl	
Methyl chavicol	1.5, 9.2	0.066	0.079	−16.8	0.011	0.037	−70.3
α−bergamotene	1.5, 9.2	0.020	0.034	−440.2	0.006	0.003	111.4
unspeciated SQT	1.5, 9.2	0.004	0.022	−83.8	0.002	0.003	−41.7

[a] Comma-separated values denote different measuring heights for hot and cold periods.
[b] See Table 5 for measurement information.
[c] Calculated as 100 · (Model – Meas)/Meas.
[d] 10^6 molec cm^{-3}.
[e] bdl = below detection limit.

ACPD
10, 21791–21866, 2010

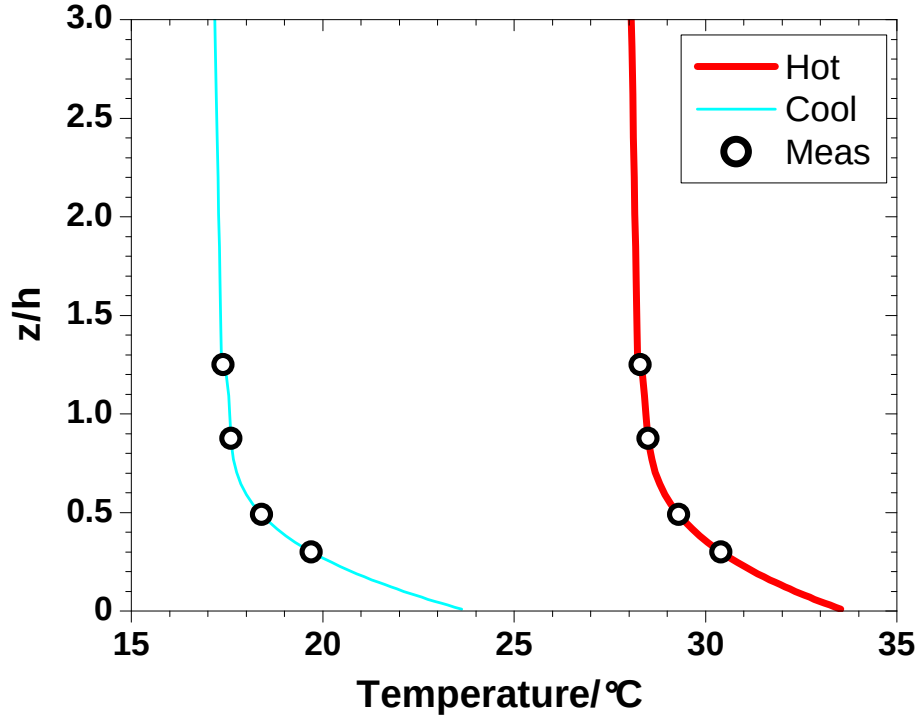

Fig. 1. Measured (open circles) and model-parameterized (solid lines) near-surface temperature profiles for the hot and cool periods.

ACPD
10, 21791–21866, 2010

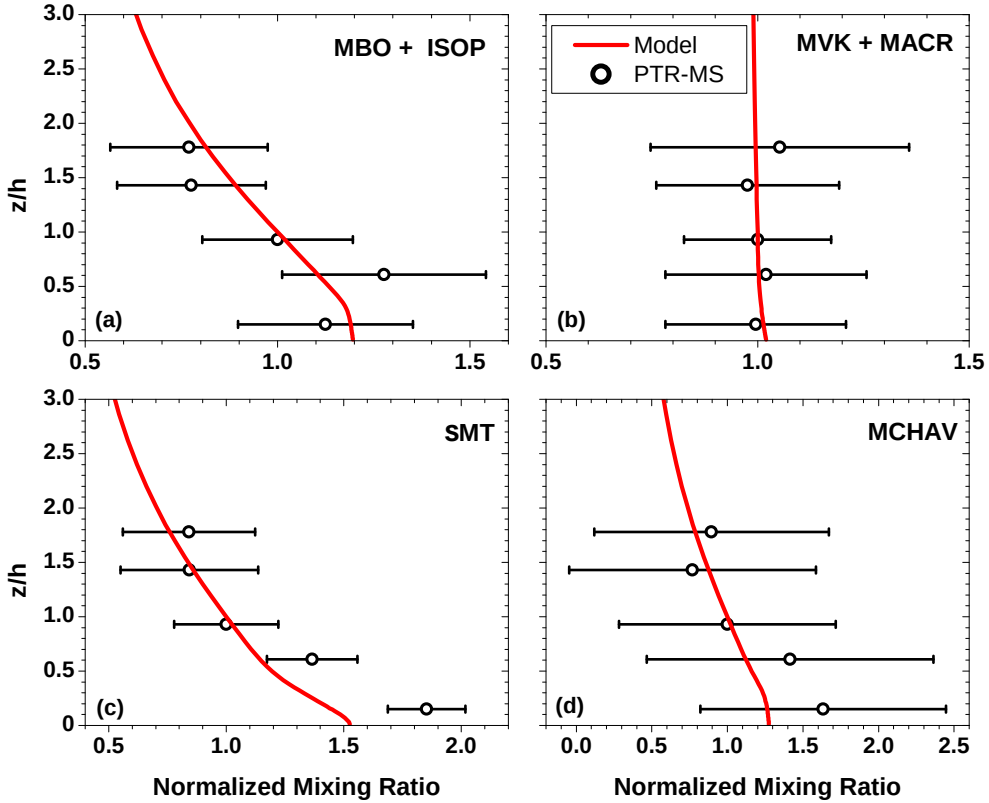

Fig. 2. Comparison of measured and modeled gradients of **(a)** the sum of MBO and isoprene, **(b)** the sum of MVK and MACR, **(c)** total monoterpenes and **(d)** methyl chavicol. Both modeled and measured values are taken from the hot period. PTR-MS observations represent the mean of six 5-minute-averaged measurements at each height and are normalized by the 9.3 m mixing ratios; error bars represent standard deviations. Model profiles are normalized to their canopy-top values ($z/h = 1$).

ACPD
10, 21791–21866, 2010

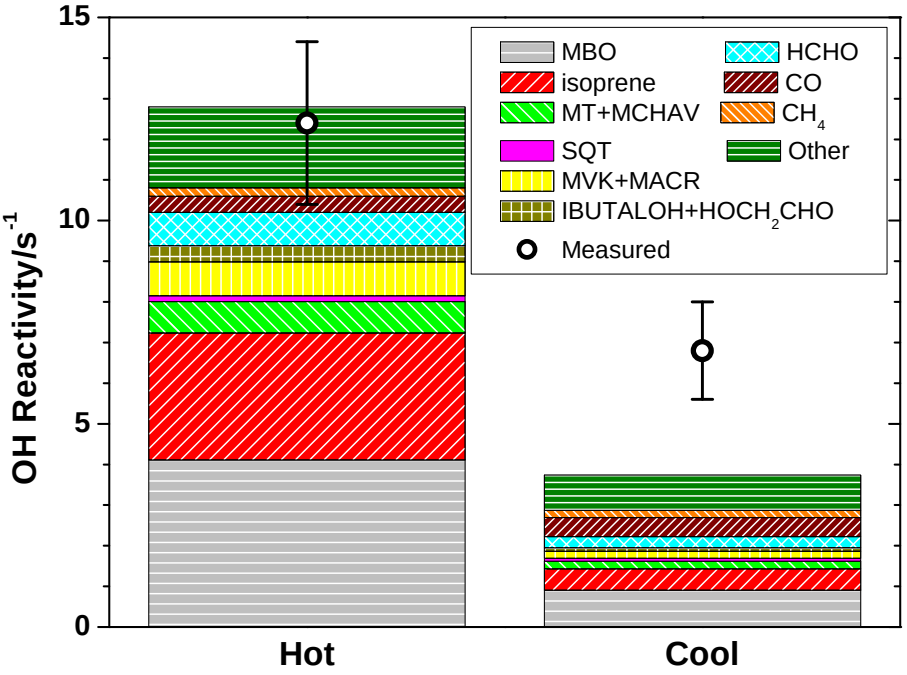

Fig. 3. Modeled OH reactivity for the hot (left) and cool (right) periods at $z/h = 1$ (10 m). The "other" category contains contributions from ~300 reactions. Open circles and error bars denote measured bulk OH reactivity (mean ± standard deviation).

ACPD
10, 21791–21866, 2010

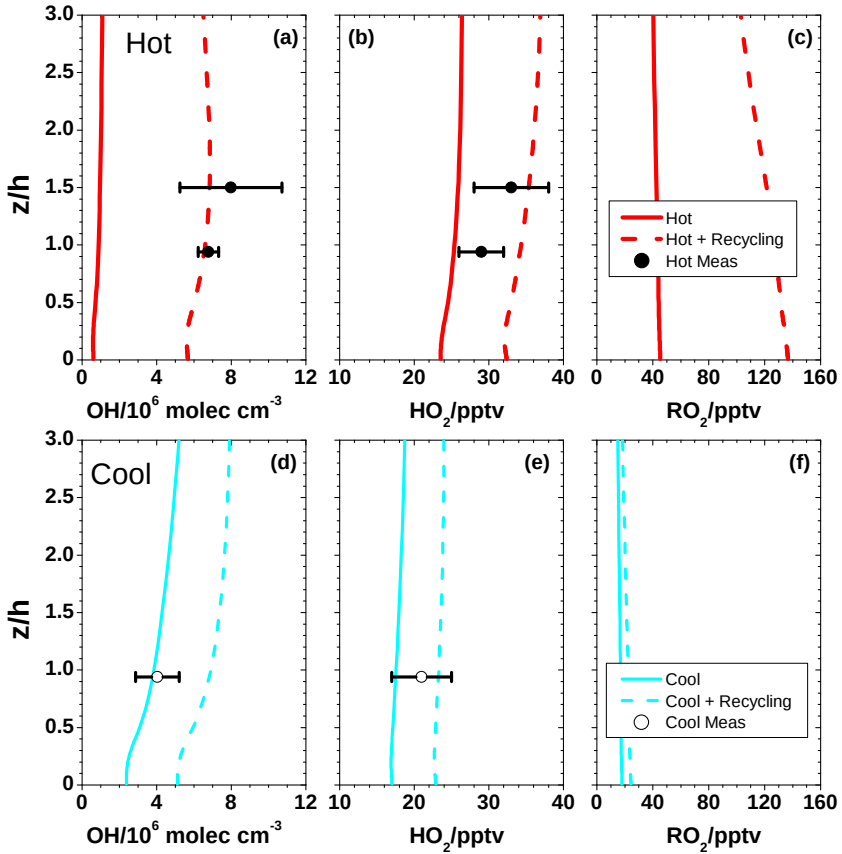

Fig. 4. Profiles of modeled OH, HO_2 and RO_2 mixing ratios during the hot **(a–c)** and cool **(d–f)** periods. Solid lines are results from model runs without the enhanced OH recycling mechanism (Sect. 3.2), while dashed lines represent model runs with OH recycling on. Filled and open circles represent observations (mean ± standard deviation) for the hot and cool periods, respectively.

ACPD
10, 21791–21866, 2010

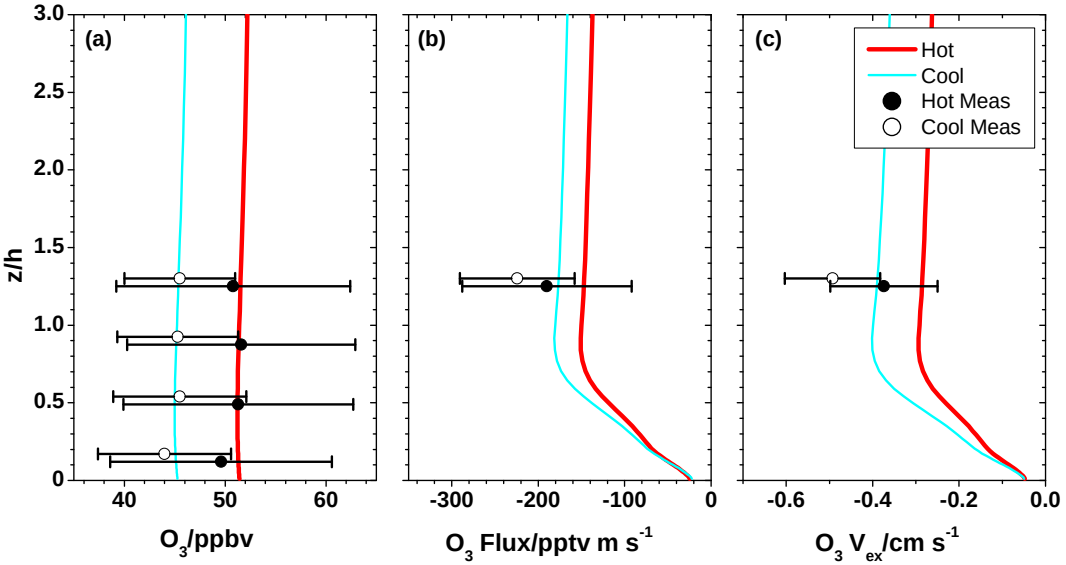

Fig. 5. Profiles of modeled ozone **(a)** mixing ratios, **(b)** fluxes and **(c)** exchange velocities for the hot and cool periods. Filled and open circles represent observations (mean ± standard deviation) for the hot and cool periods, respectively. Cool period observations are offset on the y-axis for clarity. To convert O_3 fluxes from chemical units (pptv m s^{-1}) to depositional units (µmol m^{-2} h^{-1}), multiply by 0.125.

ACPD
10, 21791–21866, 2010

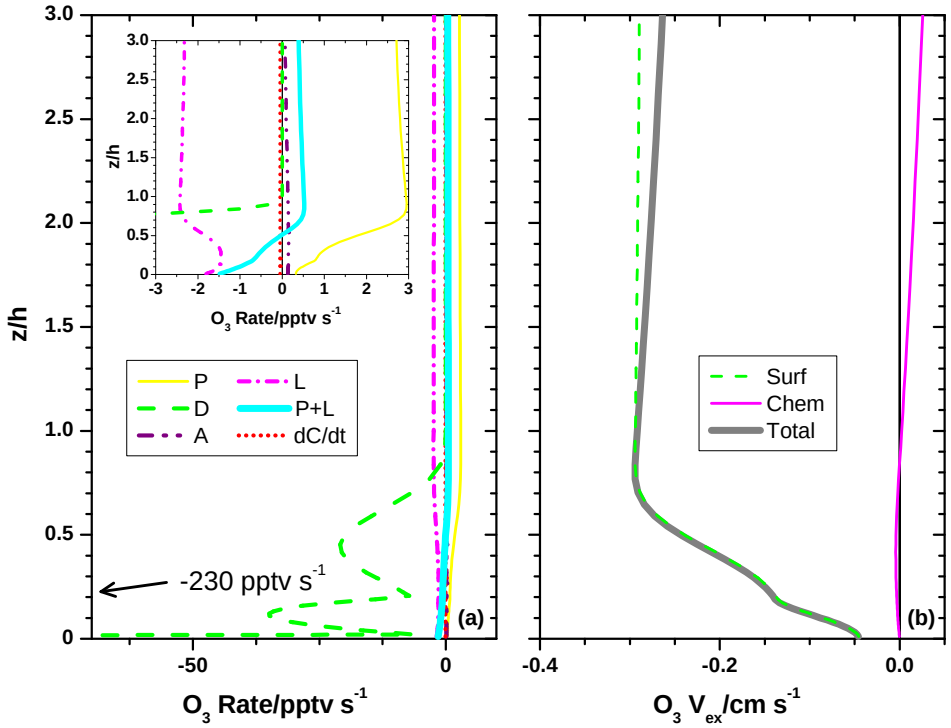

Fig. 6. **(a)** Modeled profiles of components of the instantaneous rates of change for ozone during the hot period. Contributions include chemical production (yellow solid line), chemical loss (magenta dash-dotted line), deposition (green dashed line), advection (purple dash-dot-dotted line) and storage (red dotted line). Also shown is the sum of chemical production and loss (thick cyan line). Ground deposition extends beyond the scale ($-230\,\mathrm{pptv\,s^{-1}}$). The inset provides a zoomed-in view of the same model results. **(b)** Contributions to modeled ozone exchange velocity profile for the hot period, including surface (green dashed line) and chemical (magenta solid line) processes, as well as the net exchange velocity (thick gray line).

ACPD
10, 21791–21866, 2010

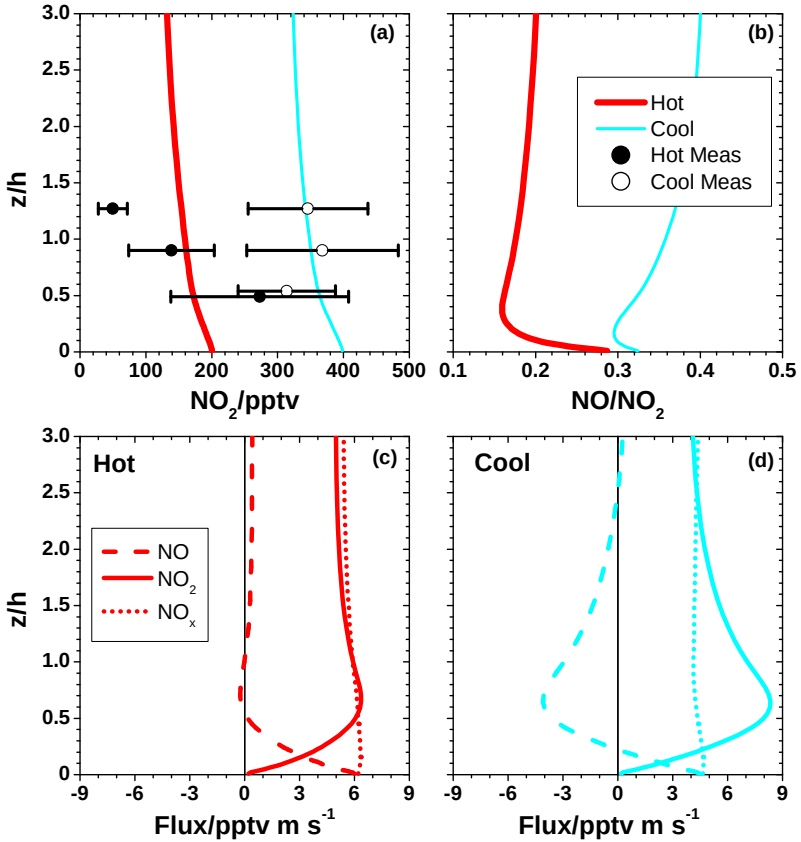

Fig. 7. **(a)** Vertical NO_2 model profiles for the hot and cool periods. Filled and open circles represent observations (mean ± standard deviation) for the hot and cool periods, respectively. The lowest cool period observation is offset on the y-axis for clarity. **(b)** Modeled NO/NO_2 ratios for the hot and cool periods. **(c)** Modeled flux profiles for NO, NO_2 and NO_x for the hot period. **(d)** As in **(c)**, but for the cool period.

ACPD
10, 21791–21866, 2010

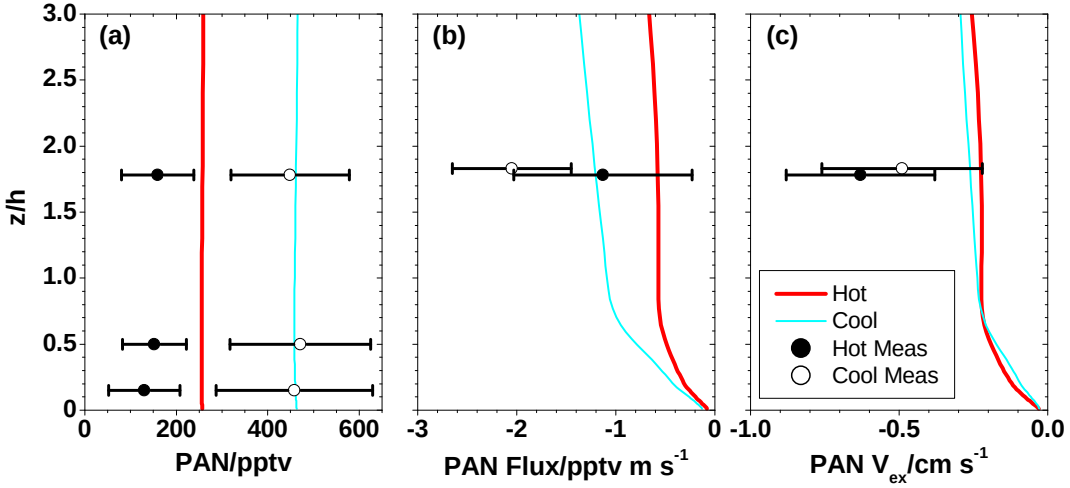

Fig. 8. Vertical profiles of **(a)** mixing ratios, **(b)** fluxes and **(c)** exchange velocities for PAN. Model results are shown for both hot and cool periods. Filled and open circles represent observations (mean ± standard deviation) for the hot and cool periods, respectively. Observations for the cool period in **(b)** and **(c)** are offset on the y-axis for clarity.

ACPD
10, 21791–21866, 2010

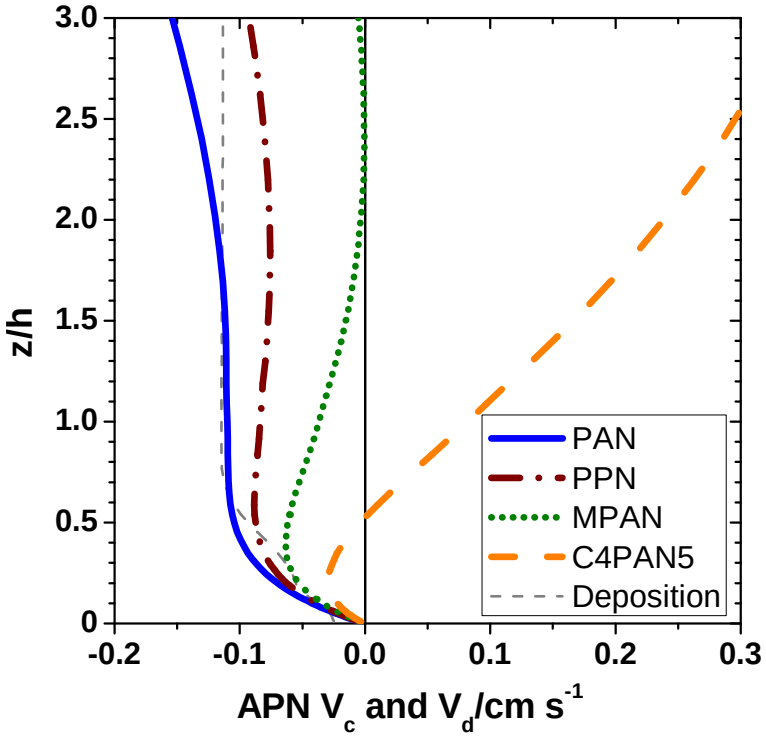

Fig. 9. Modeled chemical velocity profiles for PAN, PPN, MPAN and C4PAN5 during the hot period. The deposition velocity, which is the same for all APNs, is also shown.

ACPD
10, 21791–21866, 2010

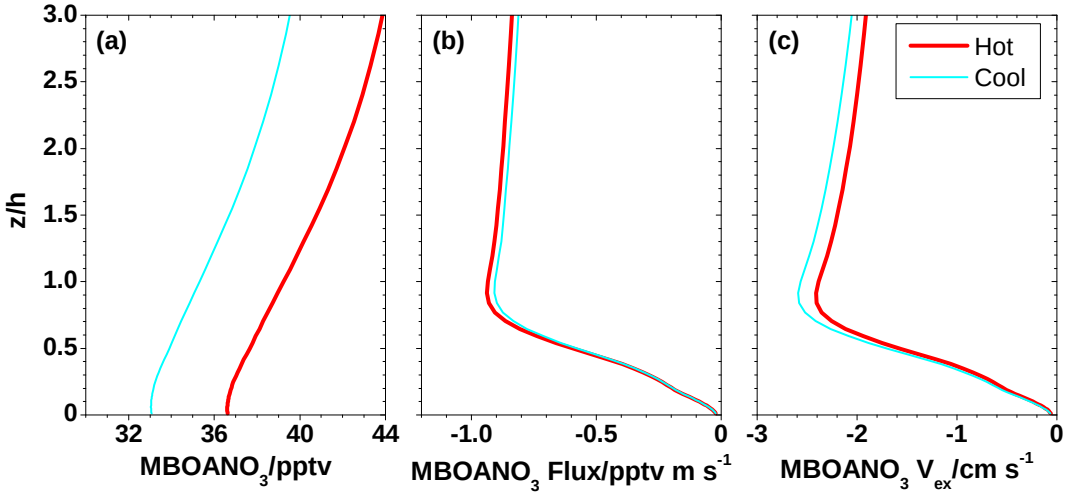

Fig. 10. Vertical profiles of **(a)** mixing ratios, **(b)** fluxes and **(c)** exchange velocities for $MBOANO_3$. Model results are shown for both hot and cool periods.

ACPD
10, 21791–21866, 2010

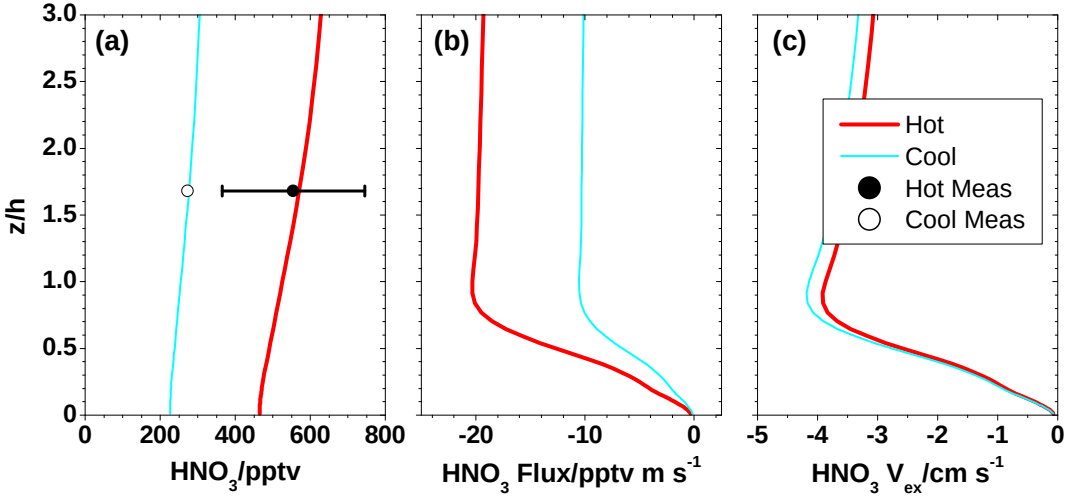

Fig. 11. Vertical profiles of **(a)** mixing ratios, **(b)** fluxes and **(c)** exchange velocities for HNO_3. Model results are shown for both hot and cool periods. Filled and open circles represent observations (mean ± standard deviation) for the hot and cool periods, respectively. The standard deviation for observed HNO_3 mixing ratios in the cool period is ± 4 pptv.

ACPD
10, 21791–21866, 2010

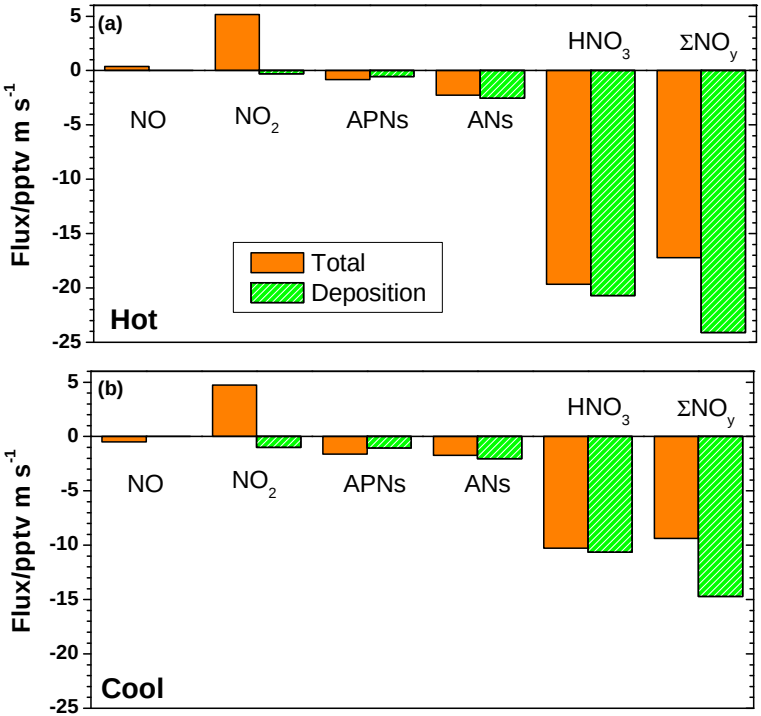

Fig. 12. Contributions of NO_y components to dry depositional (green striped bars) and net (orange solid bars) fluxes as modeled at 20 m ($z/h = 2$) for the **(a)** hot and **(b)** cool periods. To convert from pptv m s^{-1} to ngN m^{-2} s^{-1}, multiply by 0.46.

ACPD
10, 21791–21866, 2010